Cell Reports

Article

PHF7 Modulates BRDT Stability and Histone-to-Protamine Exchange during Spermiogenesis

Graphical Abstract

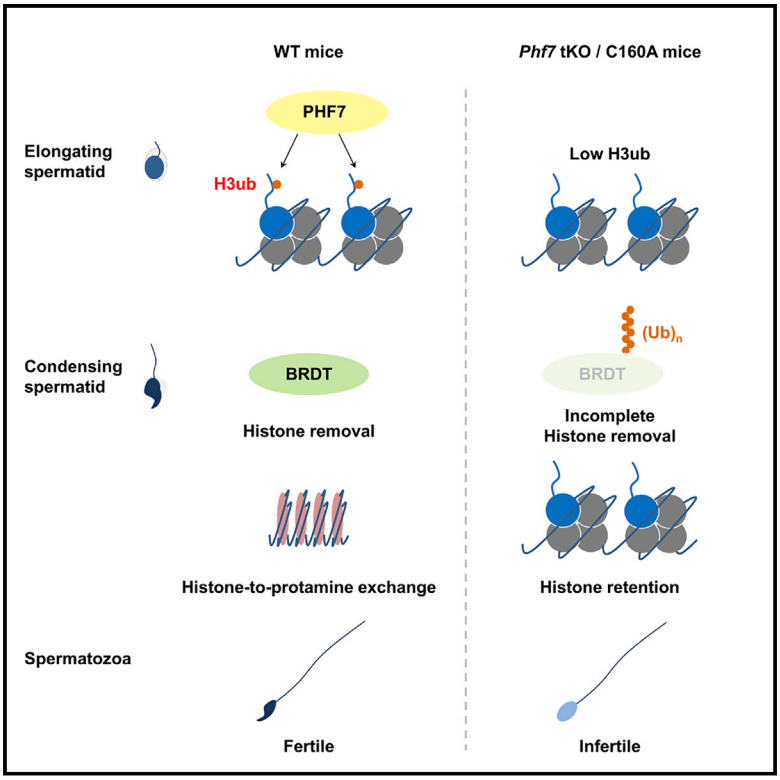

Highlights

- PHF7 is an E3 ubiquitin ligase that ubiquitinates histone H3 at lysine 14
- PHF7 is critical for histone-to-protamine exchange during spermiogenesis
- PHF7 controls BRDT stability during histone removal in early condensing spermatids
- PHF7 attenuates the ubiquitination of BRDT via histone ubiquitination

Authors

Chang Rok Kim, Taichi Noda, Hyunkyung Kim, ..., Yuki Okada, Masahito Ikawa, Sung Hee Baek

Correspondence

ikawa@biken.osaka-u.ac.jp (M.I.), sbaek@snu.ac.kr (S.H.B.)

In Brief

Histone-to-protamine exchange is essential for functional sperm. Kim et al. demonstrate that PHF7 is an E3 ubiquitin ligase for histone H3, and that PHF7-mediated histone ubiquitination regulates BRDT stability during histone removal. Mice with impaired *Phf7* show dysfunctional sperm caused by defects in histone ubiquitination and histone-to-protamine exchange.

Kim et al., 2020, Cell Reports *32*, 107950
July 28, 2020
https://doi.org/10.1016/j.celrep.2020.107950

CellPress

Cell Reports

CellPress
OPEN ACCESS

Article

PHF7 Modulates BRDT Stability and Histone-to-Protamine Exchange during Spermiogenesis

Chang Rok Kim,[1,2,10] Taichi Noda,[3,10] Hyunkyung Kim,[4] Gibeom Kim,[1,2] Seongwan Park,[5] Yongwoo Na,[2,6] Seiya Oura,[3] Keisuke Shimada,[3] Injin Bang,[2] Jun-Yeong Ahn,[1,2] Yong Ryoul Kim,[1,2] Se Kyu Oh,[1,2] Hee-Jung Choi,[2] Jong-Seo Kim,[2,6] Inkyung Jung,[5] Ho Lee,[7] Yuki Okada,[8] Masahito Ikawa,[3,9,*] and Sung Hee Baek[1,2,11,*]

[1]Creative Research Initiatives Center for Epigenetic Code and Diseases, Seoul National University, Seoul 08826, South Korea
[2]Department of Biological Sciences, Seoul National University, Seoul 08826, South Korea
[3]Research Institute for Microbial Diseases, Osaka University, Osaka 565-0871, Japan
[4]Department of Biochemistry and Molecular Biology, Korea University College of Medicine, Seoul 02841, South Korea
[5]Department of Biological Sciences, Korea Advanced Institute of Science & Technology, Daejeon 34141, South Korea
[6]Center for RNA Research, Institute for Basic Science, Seoul 08826, South Korea
[7]Graduate School of Cancer Science and Policy, Research Institute, National Cancer Center, Goyang 10408, South Korea
[8]Laboratory of Pathology and Development, Institute for Quantitative Biosciences, The University of Tokyo, Tokyo 113-0032, Japan
[9]The Institute of Medical Science, The University of Tokyo, Tokyo 108-8639, Japan
[10]These authors contributed equally
[11]Lead Contact
*Correspondence: ikawa@biken.osaka-u.ac.jp (M.I.), sbaek@snu.ac.kr (S.H.B.)
https://doi.org/10.1016/j.celrep.2020.107950

SUMMARY

Spermatogenesis is a complex process of sperm generation, including mitosis, meiosis, and spermiogenesis. During spermiogenesis, histones in post-meiotic spermatids are removed from chromatin and replaced by protamines. Although histone-to-protamine exchange is important for sperm nuclear condensation, the underlying regulatory mechanism is still poorly understood. Here, we identify PHD finger protein 7 (PHF7) as an E3 ubiquitin ligase for histone H3K14 in post-meiotic spermatids. Generation of *Phf7*-deficient mice and *Phf7* C160A knockin mice with impaired E3 ubiquitin ligase activity reveals defects in histone-to-protamine exchange caused by dysregulation of histone removal factor Bromodomain, testis-specific (BRDT) in early condensing spermatids. Surprisingly, E3 ubiquitin ligase activity of PHF7 on histone ubiquitination leads to stabilization of BRDT by attenuating ubiquitination of BRDT. Collectively, our findings identify PHF7 as a critical factor for sperm chromatin condensation and contribute to mechanistic understanding of fundamental phenomenon of histone-to-protamine exchange and potential for drug development for the male reproduction system.

INTRODUCTION

Spermatogenesis is a complex process to generate sperm possessing the half of paternal genomic information. After meiosis in which a diploid spermatocyte derived from spermatogonia is divided into four haploid spermatids, round spermatids undergo spermiogenesis to become spermatozoa, accompanied by cytosol removal, nuclear condensation, acrosome formation, and tail elongation. Compact chromatin of sperm, packaged by protamines, allows protection of genome from physical DNA damages and efficient transmission of the paternal genome to the offspring. During spermiogenesis, histones in elongating spermatids are removed from chromatin and replaced by transition proteins (TNPs) and, finally, by protamines (Wang et al., 2019a). Sperm with histone-to-protamine exchange defect show abnormal morphology and reduced motility because of the failure of nuclear condensation, leading to the difficulty in fertilization (Cho et al., 2001; Li et al., 2014b; Okada et al., 2007; Wang et al., 2016).

Prior to histone-to-protamine exchange, histone H4 hyperacetylation occurs in elongating spermatids not only for an initiation of histone removal (Goudarzi et al., 2014) but also for transcriptional regulation of spermatogenic genes (Shiota et al., 2018). Several studies have shown that many types of regulatory proteins are involved in H4 hyperacetylation. P-element induced wimpy testis in Drosophila (PIWI) regulates the localization of RNF8, which promotes ubiquitination of H2A and H2B required for H4 hyperacetylation in elongating spermatids (Gou et al., 2017; Lu et al., 2010), while the involvement of RNF8 in H4 hyperacetylation remains controversial (Sin et al., 2012). CHD5, a member of chromatin remodelers, plays roles in H4 hyperacetylation and sperm head development through transcriptional regulation (Li et al., 2014b; Zhuang et al., 2014). Following H4 hyperacetylation, Bromodomain, testis-specific (BRDT), which

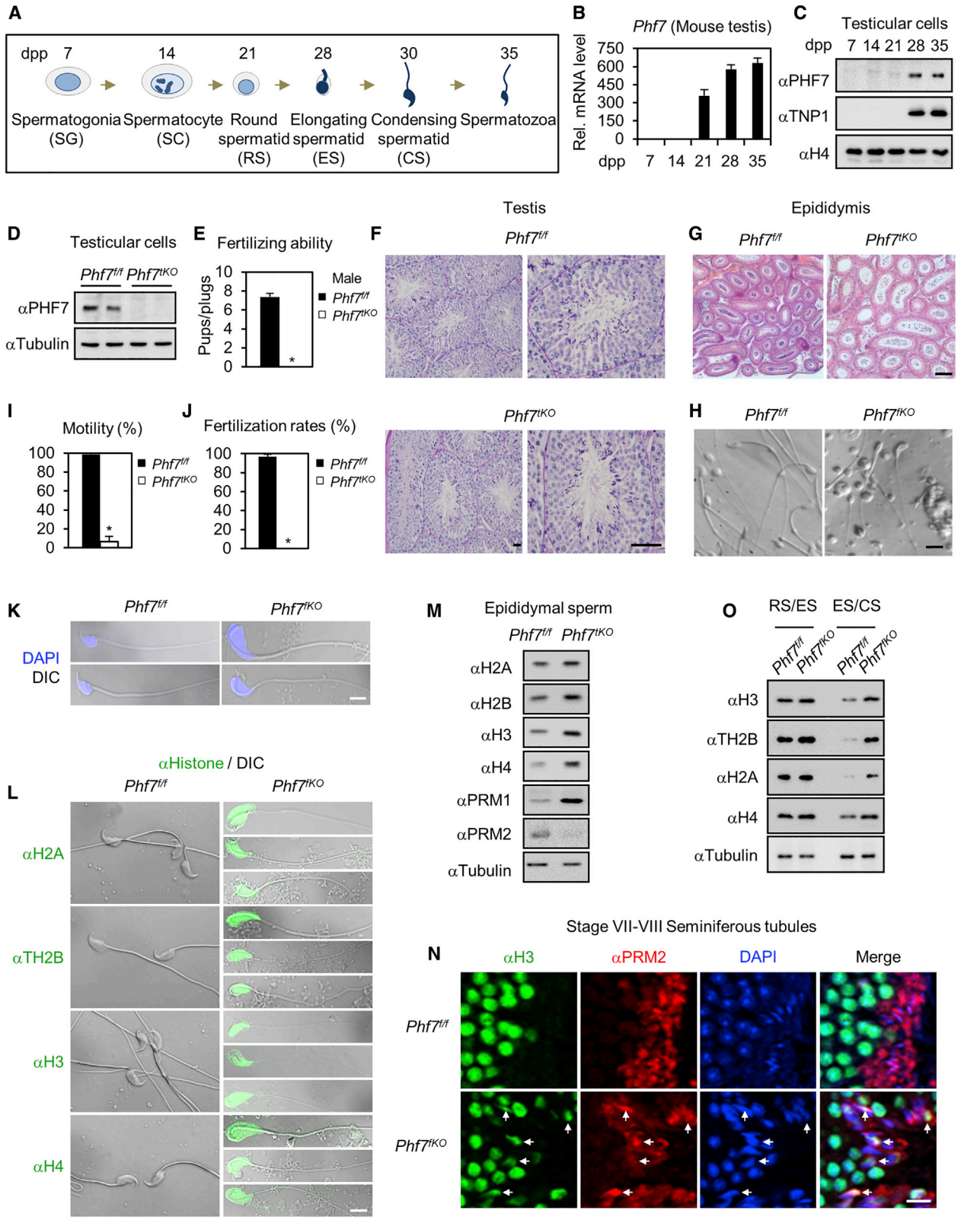

(legend on next page)

specifically binds to hyperacetylated H4 tail and reorganizes the acetylated chromatin (Dhar et al., 2012; Pivot-Pajot et al., 2003), recognizes H4K5/K8 acetylation (H4K5/K8ac) through the BD1 domain, leading to histone removal and transcriptional regulation with chromatin remodeler (Morinière et al., 2009; Pivot-Pajot et al., 2003; Sasaki et al., 2009; Wang and Wolgemuth, 2016). Recognition of acetylated chromatin by BD1 is complemented by a Bromodomain-DNA interaction (Miller et al., 2016). Moreover, PA200, a member of sperm proteasome, is required for the acetylation-associated degradation of the histones during spermiogenesis (Qian et al., 2013). However, molecular mechanisms of how histone removal is regulated during spermiogenesis have not been conducted thus far.

Among the Bromodomain and extra-terminal (BET) family, BRDT is expressed in testis specifically and has been studied as a key factor in spermatogenesis. Although several mouse models with disruption in *Brdt* gene exhibit male infertility, each model with deletion status within *Brdt* has shown defects at different stages of spermatogenesis. While *Brdt* knockout (KO) mice have defects in early spermatogenesis, *Brdt* ΔBD1 mice exhibit the failure of histone removal because of impaired binding to H4K5/K8ac, indicating that the interaction between BD1 of BRDT and acetylated H4 is crucial for spermiogenesis (Gaucher et al., 2012; Goudarzi et al., 2016). Compared with functional studies of BRDT, the regulation of BRDT has been poorly understood.

PHD finger protein 7 (PHF7) is a member of the PHF family, which has the PHD domain known as a histone methyl reader. In fly and mammals, PHF7 is expressed dominantly in testis. Especially, PHF7 is important for male sex determination of primordial germ cells (PGCs) through binding to histone H3K4me2 in fly (Yang et al., 2012). Ectopic expression of PHF7 in fly ovary induces abnormal development and tumor formation (Shapiro-Kulnane et al., 2015). Recently, it has been shown that disruption of the *Phf7* gene in mice results in spermatogenic defects and decreased H2A ubiquitination in round spermatids (Wang et al., 2019b). Here, we report that PHF7 functions as an E3 ubiquitin ligase on histone H3K14ub in post-meiotic spermatids, which maintains BRDT stability for proper histone removal during spermiogenesis.

RESULTS

Phf7^{tKO} Male Mice Exhibit Spermatogenic Defects

High expression of *Phf7* in testis led us to test whether PHF7 conducts an important role in spermatogenesis. To examine when *Phf7* is expressed during spermatogenesis, we prepared total testis extracts from mice at different developmental stages. The following developmental stages of spermatogenesis appear depending on ages: spermatogonia at 7 days postpartum (dpp), spermatocytes at 14 dpp, round spermatids at 21 dpp, elongating spermatids at 28 dpp, condensing spermatids at 30 dpp, and spermatozoa at 35 dpp (Figure 1A). *Phf7* was expressed in round and elongating spermatids as shown by increased *Phf7* mRNA level from 21 dpp (Figure 1B) and PHF7 protein level from 28 dpp (Figure 1C).

To explore the role of PHF7 in spermatogenesis, we generated *Phf7*-floxed mice (*Phf7*$^{f/f}$) from gene-targeted embryonic stem cells (ESCs) and crossed *Phf7*$^{f/f}$ mice with Stra8-Cre mice to generate testicular germ cell-specific *Phf7* KO mice (hereafter named *Phf7*^{tKO}) (Figure S1A). The protein expression of endogenous PHF7 was completely depleted in testicular cells from *Phf7*^{tKO} mice compared with *Phf7*$^{f/f}$ mice (Figure 1D). We crossed *Phf7*$^{f/f}$ or *Phf7*^{tKO} males with wild-type (WT; *Phf7*$^{+/+}$) females and found that *Phf7*^{tKO} males were infertile compared with *Phf7* $^{f/f}$ males (Figure 1E). The ratio of testis weight to body weight was comparable between *Phf7*$^{f/f}$ males and *Phf7*^{tKO} males (Figure S1B). Indeed, we could not detect the overt defects in seminiferous tubules from *Phf7*^{tKO} males by microscopic observation with hematoxylin and periodic acid-Schiff (PAS) staining (Figure 1F).

Histological analysis with hematoxylin and eosin staining on the epididymis section revealed that a lower number of sperm in tubules was observed in *Phf7*^{tKO} cauda epididymis compared

Figure 1. *Phf7*^{tKO} Male Mice Exhibit Spermatogenic Defects

(A) Schematic representation of mouse spermatogenesis.

(B) Relative *Phf7* mRNA level in testis from mice with different ages (n = 9 at 7 and 14 dpp, n = 5 at 21 dpp, n = 3 at 28 and 35 dpp). Error bars represent mean ± SEM.

(C) Protein level of PHF7 in testis from mice with different ages.

(D) Protein level of PHF7 in testicular cell extracts from *Phf7*$^{f/f}$ and *Phf7*^{tKO} mice at 8 weeks.

(E) Fertilizing ability of *Phf7*$^{f/f}$ and *Phf7*^{tKO} male mice (n = 4/group) mated with wild-type (*Phf7*$^{+/+}$) female mice. Error bars represent mean ± SD. Mann-Whitney U test, *p < 0.05.

(F) Representative histological section images of testis obtained from *Phf7*$^{f/f}$ and *Phf7*^{tKO} mice stained with hematoxylin and PAS. Scale bars, 50 μm.

(G) Representative histological section images of epididymis obtained from *Phf7*$^{f/f}$ and *Phf7*^{tKO} mice stained with hematoxylin and eosin (n = 2/group). Scale bar, 50 μm.

(H) Representative phase-contrast images of sperm from *Phf7*$^{f/f}$ and *Phf7*^{tKO} mice. Scale bar, 10 μm.

(I) Relative motility of epididymal sperm from *Phf7*$^{f/f}$ and *Phf7*^{tKO} mice (n = 4/group). Error bars represent mean ± SD. Mann-Whitney U test, *p < 0.05.

(J) *In vitro* fertilization (IVF) assay. Relative fertilization rates of sperm from *Phf7*$^{f/f}$ and *Phf7*^{tKO} mice (n = 4/group). Error bars represent mean ± SD. Mann-Whitney U test, *p < 0.05.

(K) Representative confocal images of sperm from *Phf7*$^{f/f}$ and *Phf7*^{tKO} mice with nuclei counterstained with DAPI (blue). Scale bar, 5 μm.

(L) Representative confocal images of immunostaining using anti-histone H2A, TH2B, H3, and H4 antibodies (green) in sperm from *Phf7*$^{f/f}$ and *Phf7*^{tKO} mice. Scale bar, 5 μm.

(M) Protein levels of histones and protamines in epididymal sperm extracts from *Phf7*$^{f/f}$ and *Phf7*^{tKO} mice.

(N) Representative confocal images of immunostaining with anti-H3 antibody (green), anti-PRM2 antibody (red), and DAPI (blue) on testis sections from *Phf7*$^{f/f}$ and *Phf7*^{tKO} mice (n = 2/group). Arrows indicate condensed spermatids showing simultaneous expression of H3 and PRM2. Scale bar, 10 μm.

(O) Immunoblot analysis was performed with extracts from spermatids of *Phf7*$^{f/f}$ and *Phf7*^{tKO} mice.

See also Figure S1 and Videos S1 and S2.

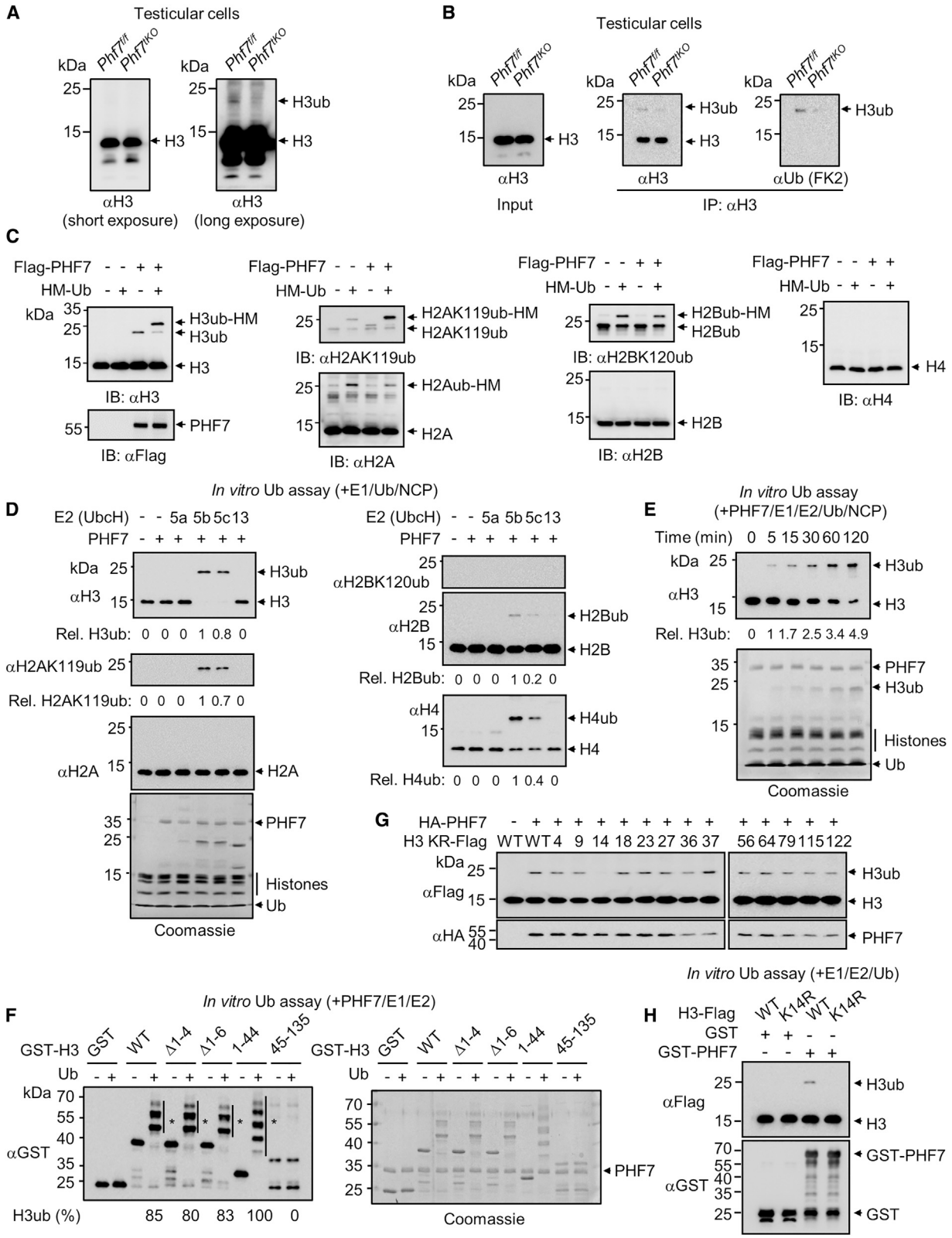

(legend on next page)

with *Phf7*$^{f/f}$ controls (Figures 1G and 1H). *Phf7*^{tKO} mice showed reduced motility of the sperm compared with *Phf7*$^{f/f}$ controls (Figure 1I; Videos S1 and S2). *In vitro* fertilization (IVF) experiments revealed that *Phf7*^{tKO} sperm showed lower fertilization rate than *Phf7*$^{f/f}$ sperm (Figure 1J). Further, we examined the sperm morphology and found that the majority of *Phf7*^{tKO} sperm had a globular and larger head with nuclei than *Phf7*$^{f/f}$ sperm (Figure 1K), indicating that *Phf7*^{tKO} sperm have less condensed chromatin in head compared with *Phf7*$^{f/f}$ controls.

Because sperm with less condensed head are caused by abnormal composition of histones and protamines in sperm chromatin, we measured the levels of histones and protamines in sperm. Immunocytochemistry and immunoblot analyses showed that higher levels of histones were detected from *Phf7*^{tKO} sperm compared with *Phf7*$^{f/f}$ controls (Figures 1L and 1M). Moreover, a higher level of PRM1 and lower level of PRM2 were observed in *Phf7*^{tKO} sperm compared with *Phf7*$^{f/f}$ controls (Figure 1M). Next, we analyzed spermatids where histone-to-protamine exchange occurs. To examine whether histones are retained in condensing/condensed spermatids where histones are not detected normally, we performed co-immunostaining of histone H3, along with PRM1, PRM2, or TNP2, on testis sections. Although H3 was not detected in condensed spermatids expressing PRM1 or PRM2 of stage VII–VIII seminiferous tubules from *Phf7*$^{f/f}$ mice, we observed spermatids showing co-expression of H3 with PRM1 or PRM2 in *Phf7*^{fKO} mice (Figures 1N and S1C). Condensing spermatids in stage I tubules of *Phf7*$^{f/f}$ mice contained TNP2 and did not exhibit H3 expression. However, H3 was co-localized with TNP2 in some condensing spermatids from *Phf7*^{fKO} mice (Figure S1D). When we analyzed protein levels of histones in spermatid fractions, spermatids of *Phf7*$^{f/f}$ mice showed a decrease in histone levels as the development progresses, whereas those of *Phf7*^{tKO} mice did not (Figure 1O). Therefore, whereas histones in condensed spermatids of *Phf7*$^{f/f}$ mice were removed, histones were retained in condensed spermatids of *Phf7*^{tKO} mice. These data indicate that *Phf7*^{tKO} males are infertile due to the defects of histone-to-protamine exchange during spermiogenesis, leading to the decrease in sperm count in a cauda epididymis and the abnormality of sperm morphology and motility.

PHF7 Is an E3 Ubiquitin Ligase for Histone H3 at Lysine 14

Unexpectedly, we found that an upward shifted band of H3 under 25 kDa was decreased in testicular cells of *Phf7*^{tKO} mice compared with those of *Phf7*$^{f/f}$ mice (Figure 2A). To test whether the shifted band is ubiquitinated H3, we performed immunoprecipitation assay using anti-H3 antibody from lysates of testicular cells followed by immunoblot analysis using anti-Ub (FK2) antibody. At the same size, ubiquitinated H3 was detected from lysates of *Phf7*$^{f/f}$ testicular cells, but the levels of ubiquitinated H3 were significantly reduced from those of *Phf7*^{tKO} testicular cells (Figure 2B).

Identification of H3 ubiquitination in spermatids allowed us to test the possibility that PHF7 functions as an E3 ubiquitin ligase of H3. Therefore, we introduced PHF7 with ubiquitin in HEK293T cells and checked PHF7-induced H3 ubiquitination. Intriguingly, we observed about 28 kDa of HisMax-Ub-H3 band, as well as about 22 kDa of shifted endogenous H3ub band, with introduction of PHF7 and HisMax-Ub (Figure 2C). Because PHF7 induces ubiquitination of H2A at K119 (Wang et al., 2019b), we observed increased H2A K119ub in the presence of PHF7. H2B and H4 were not ubiquitinated by ectopic expression of PHF7 (Figure 2C). Further, we performed *in vitro* ubiquitination assay of H3 with recombinant nucleosomes. For this, we screened potential candidate E2 ubiquitin-conjugating enzymes, including UbcH5A, UbcH5B, UbcH5C, and UbcH13, and found that UbcH5B and UbcH5C exerted H3 ubiquitination along with PHF7 as E2 enzymes *in vitro* (Figure 2D). Under the same condition, PHF7 also promoted the ubiquitination of H2A K119, H2B, and H4, but we failed to detect ubiquitination of H2B K120 using anti-H2B K120ub antibody (Figure 2D). Indeed, introduction of PHF7 with E1, UbcH5B/C, and Ub increased ubiquitination of H3 in time-dependent manner (Figure 2E). Next, we validated the site of PHF7-mediated H3 ubiquitination. *In vitro* ubiquitination assay with the deletion mutants of H3 revealed that ubiquitination occurred within N-terminal tail of H3 (Figure 2F). Liquid chromatography-tandem mass spectrometry (LC-MS/MS) on H3ub from *in vitro* ubiquitination revealed that K14 is the site of ubiquitination within H3 (Figure S2A). Moreover, mutagenesis analysis showed that only K14R mutant of H3 failed to be ubiquitinated by PHF7 (Figure 2G). The K14 site of H3 was validated by *in vitro* ubiquitination assay as well (Figure 2H). Moreover, LC-MS/MS analysis on ubiquitinated protein using lysates from PHF7-introduced HEK293T cells showed that ectopic expression of PHF7 increased the count of peptide, including modified H3K14, compared with control (Figure S2B). In LC-MS/MS analysis using testicular cells from *Phf7*$^{f/f}$ and *Phf7*^{tKO} mice, the ubiquitination of H2A and H2B was reduced about 30% by the loss of PHF7 (Figure S2C). However, LC-MS/MS analysis failed to

Figure 2. PHF7 Is an E3 Ubiquitin Ligase for Histone H3 at Lysine 14

(A) Immunoblot analysis was performed with extracts from testicular cells of *Phf7*$^{f/f}$ and *Phf7*^{tKO} mice. Long exposure data of anti-H3 immunoblot included upward shifted band of H3 under 25 kDa.

(B) Immunoprecipitation analysis was performed with lysate from testicular cells of *Phf7*$^{f/f}$ and *Phf7*^{tKO} mice.

(C) Immunoblot analysis after transfection of FLAG-tagged PHF7 and HisMax-tagged ubiquitin in HEK293T cells.

(D) *In vitro* ubiquitination assay for E2 screening with recombinant nucleosome particles (NCPs) and PHF7 proteins purified from *E. coli*. Relative histone ubiquitination levels are indicated below each immunoblot.

(E) *In vitro* ubiquitination assay with NCPs for different time points. Relative H3 ubiquitination levels are indicated below anti-H3 immunoblot.

(F) *In vitro* ubiquitination assay with deletion mutants of GST-H3 in the absence or presence of Ub. Rate of H3 ubiquitination was indicated below anti-GST immunoblot. Asterisks (*) indicate poly-ubiquitination of H3.

(G) Screening of the ubiquitination site of H3 after transfection with HA-PHF7 and C-terminal FLAG-tagged H3 KR mutants (H3 KR-FLAG) in HEK293T cells.

(H) *In vitro* ubiquitination assay with histone extracts from HEK293T cells following overexpression of C-terminal FLAG-tagged H3 WT and H3 K14R mutant.

See also Figure S2.

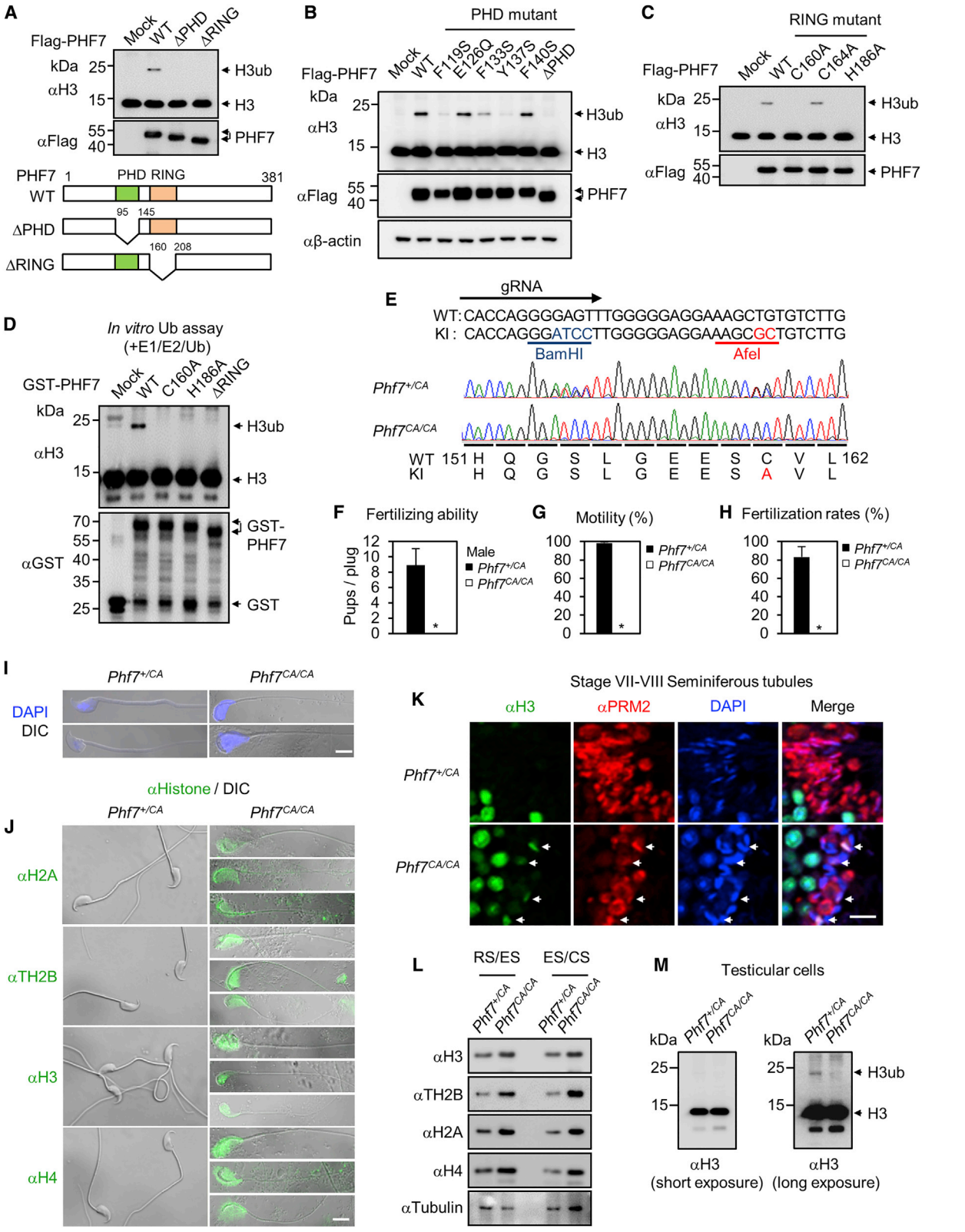

(legend on next page)

detect H3K14ub in testicular cells. This leads us to speculate that H3K14ub presents at low levels or in a small percentage of spermatids. These data indicate that PHF7 has an E3 ubiquitin ligase activity on H3 at lysine 14.

PHF7 contains both PHD domain and RING domain. Previous studies have revealed that N-terminal PHD domain of PHF7 binds H3, specifically H3K4me2, and RING domain of PHF7 is responsible for E3 ubiquitin ligase activity (Wang et al., 2019b; Yang et al., 2012). To determine whether PHD domain and/or RING domain of PHF7 are necessary for H3 ubiquitination, we generated deletion mutants for each domain and found that each domain deletion mutant failed to induce H3 ubiquitination (Figure 3A). Various PHF7 mutants with disrupted conserved residues in RING domain and PHD domain by site-directed mutagenesis led to the loss of E3 ubiquitin ligase activity of PHF7 (Figures 3B and 3C). Various RING domain mutants of PHF7 failed to ubiquitinate H3 *in vitro* (Figure 3D). Together, these data indicate that both the PHD domain and RING domain of PHF7 are required for H3 ubiquitination, and disruption of each domain led to the loss of H3 ubiquitination by PHF7.

Generation and Characterization of *Phf7* Enzymatic Dead Mutant C160A Knockin Mice

To determine whether E3 ubiquitin ligase activity of PHF7 is important for spermatogenesis, we generated *Phf7* knockin (KI) mice with C160A mutation in the RING domain of PHF7 (hereafter named $Phf7^{CA}$), which leads to the impaired enzymatic activity (Figure 3E). We crossed $Phf7^{+/CA}$ and $Phf7^{CA/CA}$ males with WT female and found that $Phf7^{CA/CA}$ males were sterile compared with $Phf7^{+/CA}$ control males (Figure 3F). $Phf7^{+/CA}$ males showed similar capacity with WT males, indicating that C160A mutation is recessive. Although none of the testis from $Phf7^{CA/CA}$ mice showed any overt microscopic defects, a smaller number of sperm was observed within the cauda epididymis from $Phf7^{CA/CA}$ mice (Figures S3A and S3B). Sperm from $Phf7^{CA/CA}$ mice showed abnormal morphology, low motility, and low capacity compared with those of $Phf7^{+/CA}$ mice (Figures 3G, 3H, and S3C; Videos S3 and S4). Similar to sperm of $Phf7^{tKO}$ mice, sperm and spermatids from $Phf7^{CA/CA}$ mice showed incomplete histone removal during spermiogenesis (Figures 3J–3L), indicating that $Phf7^{CA/CA}$ mice showed a similar phenotype with $Phf7^{tKO}$ mice. Importantly, H3 ubiquitination was reduced in testicular cells of $Phf7^{CA/CA}$ mice compared with those of $Phf7^{+/CA}$ mice (Figure 3M). Together, these data indicate that the E3 ubiquitin ligase activity of PHF7 is crucial for histone-to-protamine exchange and H3 ubiquitination during spermiogenesis.

E3 Ubiquitin Ligase Activity of PHF7 Is Crucial for Histone Removal following H4 Hyperacetylation

PHF7 in *Drosophila* has been shown to regulate the transcription of downstream genes in fly germ cells (Shapiro-Kulnane et al., 2015; Yang et al., 2017). To examine whether *Phf7* deficiency leads to genome-wide transcriptional changes in mouse spermatogenesis, we first profiled transcriptome of testicular cells from $Phf7^{f/f}$ and $Phf7^{tKO}$ mice using 10X Genomics analysis. Single-cell RNA sequencing results were highly reproducible between two biological replicates, and unsupervised clustering analysis well identified previously known multiple cell clusters from spermatogonia to spermatids (Figures 4A and S4) (Green et al., 2018; Hermann et al., 2018). Cell clustering revealed that the composition of spermatogenic cells was comparable between $Phf7^{f/f}$ and $Phf7^{tKO}$ mice. However, surprisingly, we failed to observe a meaningful difference of gene expression patterns in each cluster between $Phf7^{f/f}$ and $Phf7^{tKO}$ mice (Figure 4B), indicating that *Phf7* deficiency did not have a significant effect on transcriptome during spermatogenesis in mice. These data led us to examine chromatin condensation during spermiogenesis.

First, we began by analyzing the expression of *Tnp* and *Prm*. In supporting single-cell RNA sequencing data, qRT-PCR analysis showed little or no difference in their mRNA levels (Figure 4C). However, intriguingly, immunoblot analyses using spermatid lysates revealed significantly reduced protein levels of TNP1/2 and PRM2 in $Phf7^{tKO}$ and $Phf7^{CA/CA}$ mice compared with $Phf7^{f/f}$ and $Phf7^{+/CA}$ control mice, respectively (Figures 4D and 4E). Next, we explored H4 hyperacetylation, an epigenetic event that takes place prior to histone-to-protamine exchange in elongating spermatids. Remarkably, spermatids from $Phf7^{tKO}$ and $Phf7^{CA/CA}$ mice showed much higher levels of H4 acetylation

Figure 3. *Phf7* Enzymatic Dead C160A Knockin Mice Show Defects in Spermatogenesis and H3 Ubiquitination

(A) Schematics of PHF7 WT, ΔPHD, and ΔRING mutants. Comparison of E3 ubiquitin ligase activity of FLAG-PHF7 WT, ΔPHD, and ΔRING mutants in HEK293T cells.

(B and C) Loss of E3 ubiquitin ligase activity of PHD domain point mutants (B) or RING domain point mutants (C) of PHF7 in HEK293T cells.

(D) *In vitro* ubiquitination assay with RING domain mutants of GST-PHF7.

(E) Schematic representation of the *Phf7* C160A KI mice. KI allele possesses restriction sites of BamH I (5′-GGATTC-3′) and Afe I (5′-AGCGCT-3′).

(F) Fertilizing ability of $Phf7^{+/CA}$ and $Phf7^{CA/CA}$ male mice (n = 3/group) mated with WT ($Phf7^{+/+}$) female mice. Error bars represent mean ± SD. Mann-Whitney U test, *p < 0.05.

(G) Relative motility of epididymal sperm from $Phf7^{+/CA}$ and $Phf7^{CA/CA}$ mice (n = 3/group). Error bars represent mean ± SD. Mann-Whitney U test, *p < 0.05.

(H) IVF assay. Relative fertilization rates of sperm from $Phf7^{+/CA}$ and $Phf7^{CA/CA}$ mice (n = 3/group). Error bars represent mean ± SD. Mann-Whitney U test, *p < 0.05.

(I) Representative confocal images of sperm from $Phf7^{+/CA}$ and $Phf7^{CA/CA}$ mice with nuclei counterstained with DAPI (blue). Scale bar, 5 μm.

(J) Representative confocal images of immunostaining using anti-histone H2A, TH2B, H3, and H4 antibodies (green) in sperm from $Phf7^{+/CA}$ and $Phf7^{CA/CA}$ mice. Scale bar, 5 μm.

(K) Representative confocal images of immunostaining with anti-H3 antibody (green), anti-PRM2 antibody (red), and DAPI (blue) on testis sections from $Phf7^{+/CA}$ and $Phf7^{CA/CA}$ mice (n = 2/group). Arrow indicates condensed spermatids showing simultaneous expression of H3 and PRM2. Scale bars, 10 μm.

(L) Immunoblot analysis was performed with extracts from spermatids of $Phf7^{+/CA}$ and $Phf7^{CA/CA}$ mice.

(M) Immunoblot analysis was performed with extracts from testicular cells of $Phf7^{+/CA}$ and $Phf7^{CA/CA}$ mice. Long exposure data of anti-H3 immunoblot included H3ub band under 25 kDa.

See also Figure S3 and Videos S3 and S4.

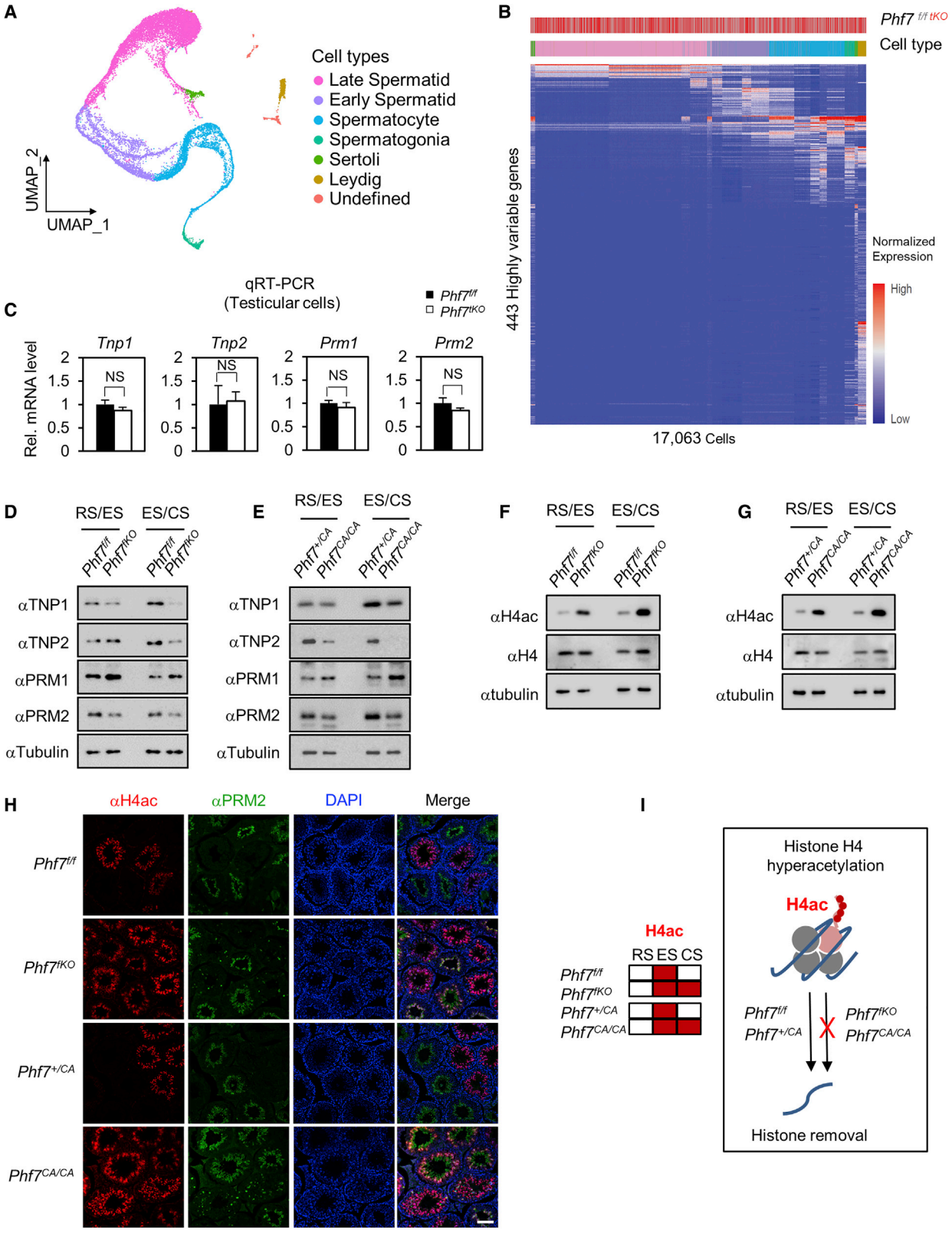

(legend on next page)

compared with those from controls (Figures 4F and 4G). To determine how disruption of *Phf7* increases H4 acetylation in testis, we performed an immunohistochemistry experiment on testis sections. The spermatogenic cycle in mice is composed of 12 stages, and stage XII is followed by stage I of the next cycle (Figure S5A) (Griswold, 2016). Following meiosis, spermiogenesis is divided into 16 steps. Spermatogonia at basal of tubule proceeds inward upon spermatogenesis; therefore, condensing (steps 12–13)/condensed (steps 14–16) spermatids are found at stage XII/stage I–VIII tubules, and elongating (steps 9–11) spermatids are located at stage IX–XI tubules. Intriguingly, although H4 acetylation in control testes appeared first in the step 9 spermatids of stage IX tubules and decreased in step 12 spermatids of stage XII tubules, H4 acetylation in $Phf7^{tKO}$ and $Phf7^{CA/CA}$ testes was intensely expressed in steps 13–16 spermatids of stage I–VIII tubules, where H4 acetylation normally disappears (Figures S5B and S5C). H4 hyperacetylation that takes place in elongating spermatids is known to induce histone removal, which results in reduced H4 acetylation level in condensing/condensed spermatids.

To validate whether H4ac is retained in condensing/condensed spermatids of $Phf7^{tKO}$ and $Phf7^{CA/CA}$ mice, we performed co-immunostaining of H4ac with TNP2 (steps 11–14 spermatids, stages XI to II), PRM1 (steps 11–16 spermatids, stages XI to VIII), or PRM2 (steps 14–16 spermatids, stages II–VIII). Whereas H4ac and PRM2 showed exclusive expression on testis sections from controls, H4ac was detected in all tubules and was co-stained with PRM2 on those of $Phf7^{tKO}$ and $Phf7^{CA/CA}$ mice (Figure 4H). Because TNP2 and PRM1 were expressed from step 11 spermatids (stage XI), H4ac was co-stained with them in only steps 11–12 spermatids (stages XI–XII) of controls. However, in $Phf7^{tKO}$ and $Phf7^{CA/CA}$ mice, H4ac was co-stained with TNP2 or PRM1 in all spermatids, expressing them due to the expression of H4ac in all tubules (Figures S6A and S6B). Because we observed retained histones in condensing/condensed spermatids from $Phf7^{tKO}$ and $Phf7^{CA/CA}$ mice, H4ac was also retained.

To examine the relationship between PHF7 and H4ac, we generated N-terminal FLAG-tagged *Phf7* knockin mice (hereafter named $Phf7^{FLAG}$) (Figure S7A). Immunoblot analysis using testicular cells from $Phf7^{FLAG/+}$ mice confirmed expression of FLAG-PHF7 protein (Figure S7B). When we performed immunohistochemistry with anti-FLAG antibody, FLAG-PHF7 was detected from stage XI tubules to stage II tubules and within the nucleus of steps 11–12 spermatids (stages XI–XII) (Figures S7C and S7D). Co-immunostaining of H4ac and FLAG on testis sections from $Phf7^{FLAG/+}$ mice demonstrated that FLAG-PHF7 was expressed after the induction of H4ac and was co-localized with H4ac in steps 11–12 spermatids (stages XI–XII) (Figure S7E). The expression timing of PHF7 indicates that loss of PHF7 does not affect the initiation of H4 hyperacetylation. Taken together, we conclude that abnormally retained H4 acetylation in condensing/condensed spermatids from $Phf7^{tKO}$ and $Phf7^{CA/CA}$ mice is derived from the incomplete histone removal during spermiogenesis. These data indicate that $Phf7^{tKO}$ and $Phf7^{CA/CA}$ mice have defects in histone removal following H4 hyperacetylation (Figure 4I).

Inactivation of PHF7 Causes Downregulation of BRDT in Early Condensing Spermatids

To further explore the molecular mechanism of why histone removal following H4 hyperacetylation is impaired in $Phf7^{tKO}$ and $Phf7^{CA/CA}$ mice, we first checked the level of BRDT, which is known as histone removal factor that recognizes H4 acetylation. Surprisingly, spermatids from $Phf7^{tKO}$ or $Phf7^{CA/CA}$ mice showed lower protein level of BRDT than those of $Phf7^{f/f}$ or $Phf7^{+/CA}$ mice with no significant difference in mRNA levels of *Brdt* between them (Figures 5A and 5B). To examine which spermatogenic stage BRDT is decreased in $Phf7^{tKO}$ or $Phf7^{CA/CA}$ mice, we performed immunohistochemistry for BRDT and H4ac. Given that BRDT can be detected from spermatocytes to elongating spermatids in mice or spermatozoa in human (Berkovits and Wolgemuth, 2013), we found that BRDT was expressed until step 12 spermatids (stage XII), and its expression was decreased in step 13 spermatids (stage I) of $Phf7^{f/f}$ or $Phf7^{+/CA}$ mice (Figures 5C and 5D). H4ac was co-stained with BRDT in the nuclei of step 11 spermatids (stage XI) and step 12 spermatids (stage XII), and their levels decreased together in the nuclei of step 13 spermatids (stage I) (Figure 5E). In $Phf7^{tKO}$ or $Phf7^{CA/CA}$ mice, because BRDT was detected diffusively in the nuclei of step 11 spermatids (stage XI) and with lower levels in the nuclei of step 12 spermatids (stage XII), relatively more remnant of H4ac was observed in the nuclei of step 12 spermatids (stage XII) and step 13 spermatids (stage I) compared with controls (Figures 5C–5E). Moreover, H4ac was enriched in certain parts of the nuclei of step 11 spermatids (stage XI) from $Phf7^{tKO}$ or $Phf7^{CA/CA}$ mice, while H4ac was distributed throughout the nuclei of those from controls (Figures 5C and 5D). Histone is removed from late

Figure 4. E3 Ubiquitin Ligase Activity of PHF7 Is Crucial for Histone Removal following H4 Hyperacetylation

(A and B) t-distributed stochastic neighbor embedding (t-SNE) analysis of testicular cells from both genotypes colored by annotated cell types (A), and normalized expression level of highly variable genes in all cells (B) obtained from single-cell RNA sequencing analysis. Both genes and cells in the heatmap are clustered using Euclidean distance. Metadata of each cell are plotted above the heatmap; genotype ($Phf7^{f/f}$, gray; $Phf7^{tKO}$, red) from experimental information and cell type from t-SNE analysis.

(C) Relative mRNA levels of *Tnp1/2* and *Prm1/2* in testicular cells from $Phf7^{f/f}$ and $Phf7^{tKO}$ mice (n = 3/group). Error bars represent mean ± SEM. Student's t test was used. NS, non-significant.

(D) Immunoblot analysis on TNPs and PRMs was performed with extracts from spermatids of $Phf7^{f/f}$ and $Phf7^{tKO}$ mice.

(E) Immunoblot analysis on TNPs and PRMs was performed with extracts from spermatids of $Phf7^{+/CA}$ and $Phf7^{CA/CA}$ mice.

(F) Immunoblot analysis on H4ac and H4 was performed with extracts from spermatids of $Phf7^{f/f}$ and $Phf7^{tKO}$ mice.

(G) Immunoblot analysis on H4ac and H4 was performed with extracts from spermatids of $Phf7^{+/CA}$ and $Phf7^{CA/CA}$ mice.

(H) Representative confocal images of immunostaining with anti-H4ac antibody (red), anti-PRM2 antibody (green), and DAPI (blue) on testis sections from $Phf7^{f/f}$, $Phf7^{tKO}$, $Phf7^{+/CA}$, and $Phf7^{CA/CA}$ mice (n = 2/group). Scale bar, 100 μm.

(I) Schematic model of PHF7 function in histone removal following H4 hyperacetylation.

See also Figures S4–S7.

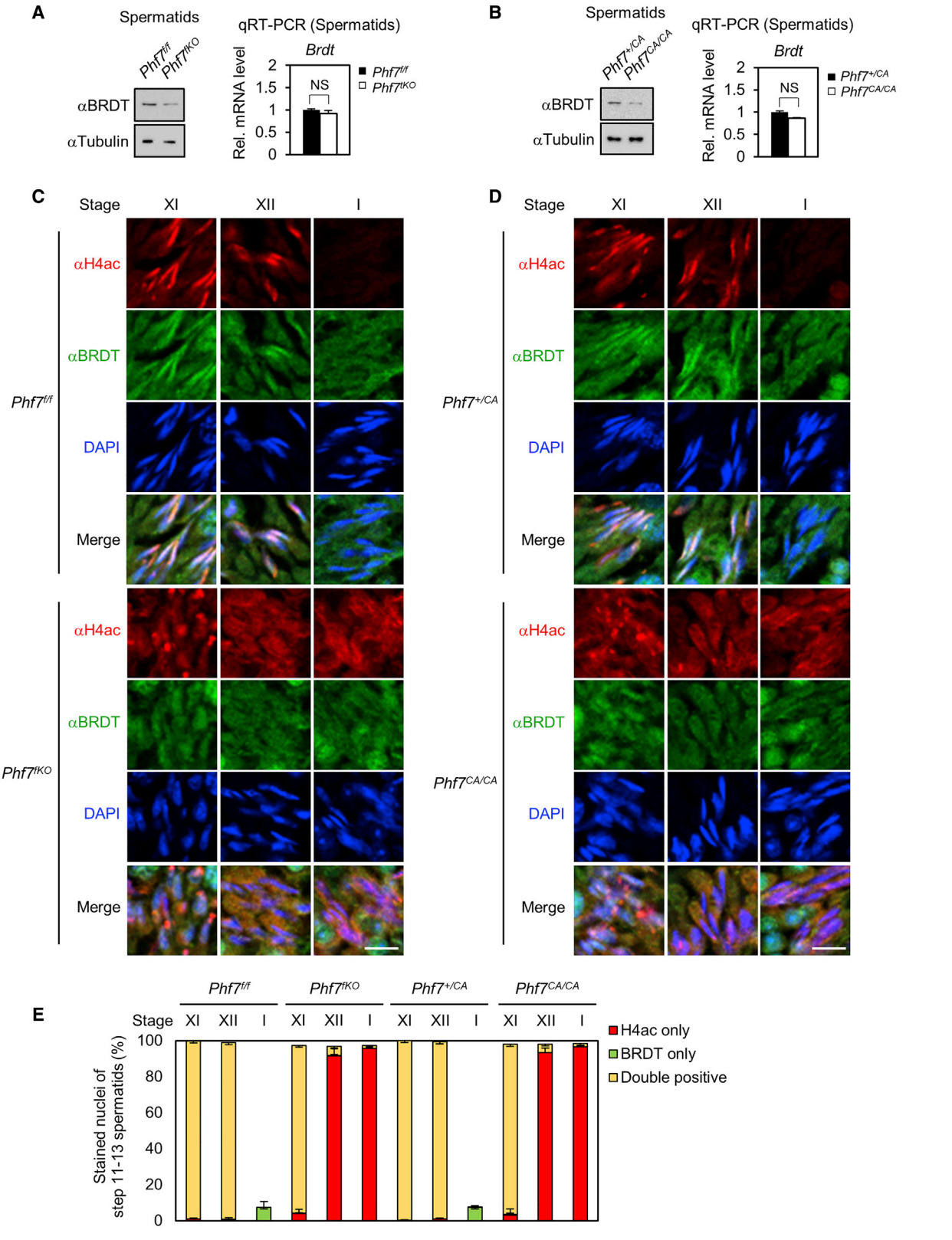

(legend on next page)

elongating spermatids to early condensing spermatids, and H4ac is not detected in step 13 spermatids (stage I) (Shirakata et al., 2014; Wang et al., 2019a). These data indicate that co-expression of H4ac and BRDT until step 12 spermatids is crucial for histone removal, and E3 ubiquitin ligase activity of PHF7 is required for proper distribution of H4ac and maintenance of BRDT levels in the nuclei of steps 11–12 spermatids. Therefore, we conclude that the impairment of PHF7 leads to failure in maintaining BRDT levels in step 12 spermatids and then results in incomplete histone removal.

E3 Ubiquitin Ligase Activity of PHF7 on Histone Is Crucial for Maintaining BRDT Stability

To test the possibility that PHF7 is associated with BRDT in post-meiotic spermatids, we first examined the co-expression of PHF7 and BRDT in spermatids from *Phf7*$^{FLAG/+}$ mice. Immunohistochemistry analysis showed that PHF7 and BRDT were co-expressed in steps 11–12 spermatids (stage XI–XII) (Figure 6A). The BET family proteins, including BRD2, BRD3, and BRD4, have a conserved SPOP (Speckle-type POZ protein) degron sequence between BD1 and BD2, and their stability is regulated by Cul3^{SPOP} E3 ubiquitin ligase (Dai et al., 2017; Janouskova et al., 2017; Zhang et al., 2017). Importantly, we found that BRDT possesses conserved SPOP degron sequence (Figure 6B). Immunoblot analysis following introduction of both BRDT and SPOP into HEK293T cells revealed the SPOP-mediated degradation of BRDT was inhibited by MG132 treatment (Figure 6C). BRDT mutant with deletion of SPOP degron sequence (BRDT ΔD) was not affected by SPOP, indicating that Cul3^{SPOP} E3 ubiquitin ligase is responsible for degradation of BRDT.

To test whether PHF7 affects BRDT stability, we introduced BRDT, SPOP, and PHF7 into HEK293T cells. PHF7 WT increased BRDT protein level by attenuating SPOP-mediated degradation of BRDT, whereas PHF7 C160A mutant failed to do so (Figure 6D). BRD4 and PTEN (Li et al., 2014a), the known substrates of SPOP, were not upregulated by the introduction of PHF7, indicating that PHF7 did not affect SPOP activity. Both SPOP and Cul3 were expressed in spermatids, and the levels of BRD4 and PTEN in spermatids containing inactive PHF7 were comparable with controls (Figures 6E). Then, ubiquitination assay revealed that PHF7 WT, but not PHF7 C160A mutant, attenuated the ubiquitination of BRDT (Figure 6F). Immunocytochemistry assay showed that BRDT, SPOP, and PHF7 were co-localized in the nucleus (Figure 6G). *In vitro* ubiquitination assay revealed that the incorporation of PHF7 did not attenuate SPOP-induced ubiquitination of BRDT (Figure 6H), indicating that PHF7 does not directly regulate ubiquitination of BRDT. Taken together, these data indicate that the E3 ubiquitin ligase activity of PHF7 is critical for maintaining BRDT stability by attenuating the degradation of BRDT by SPOP.

To clarify how PHF7 affects BRDT protein stability, we next checked the binding between PHF7 and BRDT. Unexpectedly, PHF7 failed to bind BRDT directly (Figure 7A), and this led us to examine whether PHF7-mediated histone ubiquitination is linked to regulation of BRDT. *In vitro* pull-down assay with GST-BRDT and nucleosome bearing histone ubiquitination and/or H4ac revealed that PHF7-mediated histone ubiquitination slightly augmented binding of BRDT with nucleosome bearing H4ac (Figure 7B). Nevertheless, nucleosome bearing PHF7-mediated histone ubiquitination and H4ac suppressed SPOP-induced ubiquitination of BRDT *in vitro*, unlike nucleosome bearing only one of the modifications (Figure 7C). These data indicate that PHF7-mediated histone ubiquitination interacts with BRDT and modulates its ubiquitination in the presence of H4ac. We speculate that BRDT recognizes H4ac following H4 hyperacetylation from elongating spermatids, and then PHF7-mediated histone ubiquitination contributes to the stabilization of BRDT for facilitating histone removal in early condensing spermatids (Figure 7D).

DISCUSSION

PHF7 ortholog in *Drosophila* has been shown to control male sex determination by activating male-specific gene expression in early germ cells (Yang et al., 2012). In mice, previous studies have focused on PHF7-mediated H2Aub in round spermatids, which may be followed by RNF8-mediated H2Aub and H2Bub in elongating spermatids, a process required for histone-to-protamine exchange (Wang et al., 2019b). Here, we find that H3K14 is another substrate of PHF7, and H3ub is reduced in testicular cells from mice with impaired *Phf7*. Following H4 hyperacetylation in elongating spermatids, PHF7-mediated histone ubiquitination combined with H4ac contributes to stabilization of BRDT, and thus PHF7 plays a key role in maintaining BRDT stability in early condensing spermatids. Disruption of *Phf7* causes decreased histone ubiquitination followed by decreased protein levels of BRDT in early condensing spermatids, leading to histone retention in defective sperm. We suggest that enrichment of BRDT on chromatin via histone ubiquitination facilitates histone removal for histone-to-protamine exchange.

Several mouse models have advanced our understanding on histone-to-protamine exchange. The spermatogenic defects of *Phf7*^{tKO} and *Phf7*$^{CA/CA}$ mice are similar to *Brdt* ΔBD1 mice, which show male infertility, reduced number of sperm, abnormal morphology of sperm, and retained histones in sperm (Gaucher et al., 2012; Shang et al., 2007). Given that BD1 of BRDT recognizes H4ac for histone removal, the failure of histone removal following H4 hyperacetylation in *Phf7*^{tKO} and *Phf7*$^{CA/CA}$ mice may be because of reduced BRDT expression in early condensing spermatids. Given that *Phf7*^{tKO} and *Phf7*$^{CA/CA}$

Figure 5. PHF7 Is Responsible for Maintaining BRDT Levels in Early Condensing Spermatids

(A and B) The protein levels of BRDT and relative mRNA levels of *Brdt* in spermatids from *Phf7*$^{f/f}$ and *Phf7*^{tKO} mice (n = 3/group) (A) or *Phf7*$^{+/CA}$ and *Phf7*$^{CA/CA}$ mice (n = 3/group) (B). Error bars represent mean ± SEM. Student's t test was used. NS, non-significant.

(C and D) Representative confocal images of immunostaining with anti-H4ac antibody (red), anti-BRDT antibody (green), and DAPI (blue) on testis sections from *Phf7*$^{f/f}$ and *Phf7*^{tKO} mice (n = 2/group) (C) or *Phf7*$^{+/CA}$ and *Phf7*$^{CA/CA}$ mice (n = 2/group) (D). Roman numerals indicate the spermatogenic stages of seminiferous tubule. Scale bars, 10 μm.

(E) Quantification on the stained nuclei of elongating or condensing spermatids for H4ac and/or BRDT. Error bars represent mean ± SD.

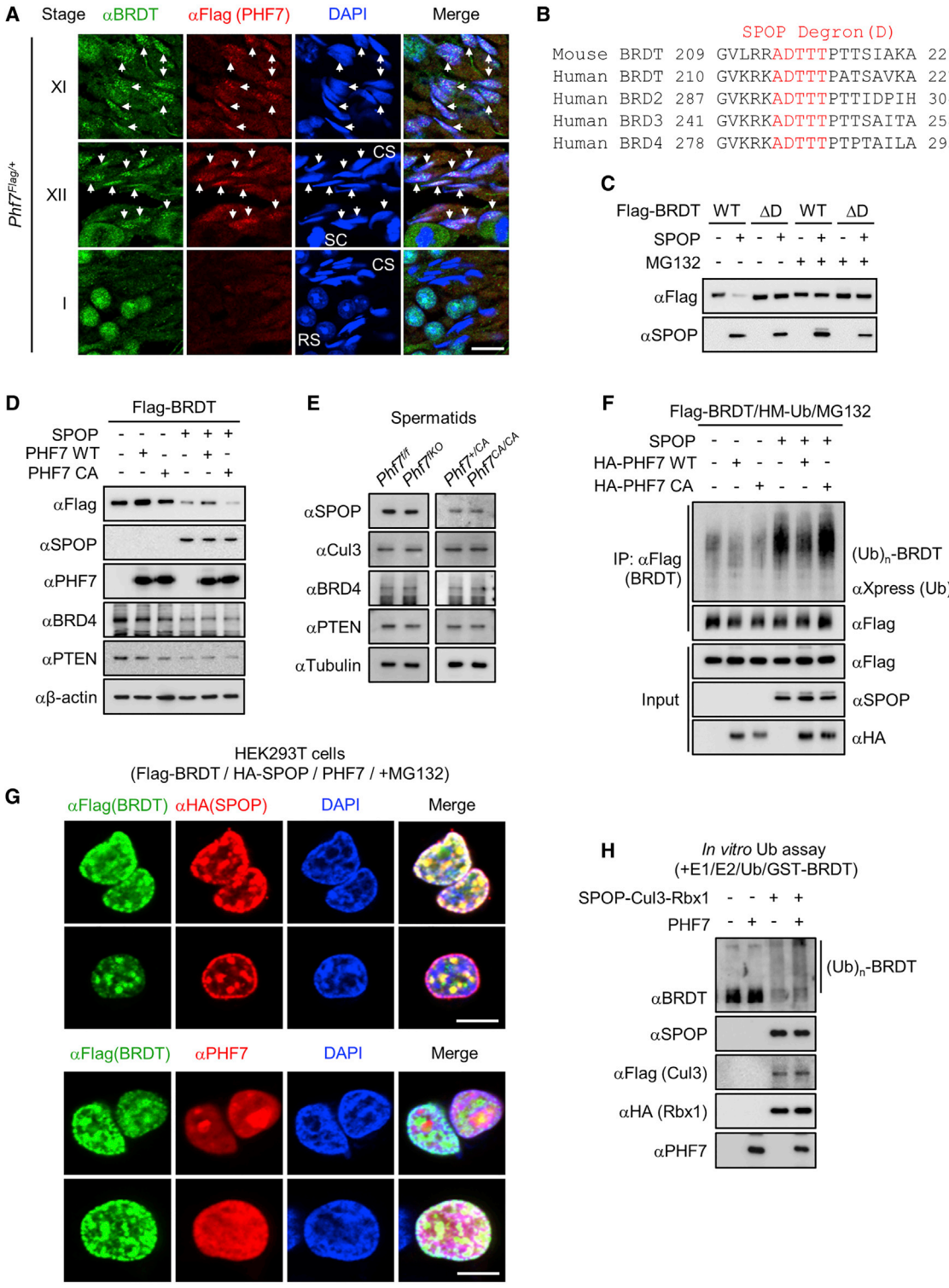

Figure 6. E3 Ubiquitin Ligase Activity of PHF7 Regulates BRDT Stability

(A) Representative confocal images of immunostaining with anti-BRDT antibody (green), anti-FLAG antibody (red), and DAPI (blue) on testis sections from *Phf7*$^{FLAG/+}$ mice (n = 2). Roman numerals indicate the spermatogenic stages of seminiferous tubule. Arrows indicate the nucleus (DAPI) of spermatids showing simultaneous expression of BRDT and FLAG-PHF7. Scale bar, 10 μm.

(B) Conserved SPOP degron (D) sequence in BET family.

(legend continued on next page)

mice have defects in protein expression of TNP and PRM, while their mRNA levels were not changed, it is plausible that PHF7 may be required for protein expression of not only BRDT but also TNPs and PRMs. *H2A.L.2* KO mice showed abnormal assembly and processing of TNPs and PRMs on chromatin without alteration of their protein levels (Barral et al., 2017). According to a previous model showing that histones are removed after loading and assembly of TNPs/PRMs, it is tempting to speculate that PHF7 may work on process following H2A.L.2.-associated TNP/PRM loading on chromatin.

BRDT is expressed first in early spermatocytes and has multiple functions depending on developmental stages (Gaucher et al., 2012). Previous studies have shown that transcription in round spermatids begins to be repressed from early spermiogenesis, resulting in shutdown of all transcription in spermatozoa (Green et al., 2018; Hermann et al., 2018). BRDT is involved in transcriptional regulation prior to repression of transcription in early elongating spermatids and histone removal through binding H4ac in late elongating spermatids (Goudarzi et al., 2016). Single-cell RNA sequencing analysis using testicular cells reveal that *Phf7* deficiency does not affect transcriptome. *In vitro* Br-UTP run-on assay tracking global transcriptional status indicates that transcription occurs until step 9 spermatids (Xia et al., 2012). Given that PHF7 is expressed in steps 11–14 spermatids as shown in $Phf7^{FLAG/+}$ mice, PHF7 may function after entire transcriptional activity is repressed. Moreover, *Phf7* deficiency affects the reduction of BRDT in step 12 spermatid where histone removal occurs. Therefore, we conclude that PHF7-mediated regulation of BRDT works for histone removal after transcriptional repression.

The PHF family is known as a reader recognizing histone methylation through PHD domains, and can recruit transcriptional regulators and induce histone modifications. PHF1 and PHF19 are components of the PRC2 complex, and they recognize H3K36me3 through their Tudor domain in ESCs (Cai et al., 2013). PHF2 and PHF8 contain the JmjC domain, which plays an important role in histone demethylation. PHF2 demethylates H3K9me1/2, and PHF8 demethylates H3K9me1/2 and H4K20me1 (Baba et al., 2011; Liu et al., 2010; Qi et al., 2010; Wen et al., 2010). Moreover, some PHFs have intrinsic E3 ubiquitin ligase activities. PHF15/Jade-2 induces ubiquitination of LSD1 upon neuronal differentiation, and PHF17/Jade-1 inhibits Wnt signaling by promoting ubiquitination of β-catenin (Chitalia et al., 2008; Han et al., 2014). PHF7 is a RING-type E3 ubiquitin ligase containing individual substrate binding domain and catalytic domain. Although the N-terminal PHD domain of PHF7 turned out to be a reader for H3K4me2 (Yang et al., 2012), whether the interaction between the PHD domain of PHF7 and H3K4me2 is required for PHF7-mediated H3 ubiquitination is still obscure. First, PHF7 can ubiquitinate H3 mutants that are incapable of H3K4 methylation. Second, mutation in the PHD domain of PHF7 led to the reduced H3 ubiquitination compared with PHF7 WT. Finally, the N-terminal tail (1–44 aa) of H3 is sufficient for PHF7-mediated H3 ubiquitination, which provides both the ubiquitination site (K14) and the PHF7 binding region. Therefore, in the case of H3 ubiquitination, the PHD domain of PHF7 may interact with other regions within the N-terminal tail of H3 instead of H3K4me2.

Because the E3 ubiquitin ligase activity of PHF7 is required for spermiogenesis, PHF7 could be a diagnostic indicator of male infertility examination and potential target of male contraceptive drug. JQ1, an inhibitor of the BRD family, was suggested as a male contraceptive drug by targeting BRDT in mice (Matzuk et al., 2012). However, JQ1 inhibits ubiquitously expressed BRD2, BRD3, and BRD4, which still have risk of side effects. PHF7 is expressed in post-meiotic spermatids dominantly and works at late spermatogenesis, while BRDT begins to function from early spermatogenesis. Our results indicate that inhibition of E3 ubiquitin ligase activity of PHF7 on histone ubiquitination may abrogate BRDT stabilization and roles of BRDT in histone removal without affecting transcriptional roles of BRDT. Thus, specific inhibition of PHF7 using small molecules may have a profound effect on male contraception. Our finding of PHF7 function will contribute to mechanistic understanding of the fundamental phenomenon of histone-to-protamine exchange and potential for drug development for the male reproduction system.

STAR★METHODS

Detailed methods are provided in the online version of this paper and include the following:

- KEY RESOURCES TABLE
- RESOURCE AVAILABILITY
  - Lead Contact
  - Materials Availability
  - Data and Code Availability
- EXPERIMENTAL MODEL AND SUBJECT DETAILS
  - Generation of Phf7 conditional knock-out mice
  - Generation of Phf7 C160A knock-in mice and Flag-tagged Phf7 knock-in mice
  - Cell culture
- METHOD DETAILS
  - Antibodies and reagents
  - Sperm motility
  - *In vitro* fertilization assay
  - Histology

(C) Immunoblot analysis after transfection with FLAG-BRDT (1–555 aa) wild-type, ΔD mutant, and SPOP in HEK293T cells in the absence or presence of MG132 treatment.
(D) Immunoblot analysis after transfection with FLAG-BRDT, SPOP, PHF7 wild-type, and C160A mutant in HEK293T cells.
(E) The protein levels of SPOP, Cul3, BRD4, and PTEN in spermatids from $Phf7^{f/f}$ and $Phf7^{tKO}$ mice or $Phf7^{+/CA}$ and $Phf7^{CA/CA}$ mice.
(F) Ubiquitination assay after introduction of FLAG-BRDT, SPOP, PHF7 wild-type, and C160A mutant in HEK293T cells upon MG132 treatment.
(G) Representative confocal images of immunostaining with anti-HA or PHF7 antibody (red), anti-FLAG antibody (green), and DAPI (blue) on transfected HEK293T cells. Scale bars, 10 μm.
(H) *In vitro* ubiquitination assay with BRDT, SPOP-Cul3-Rbx1, and PHF7.

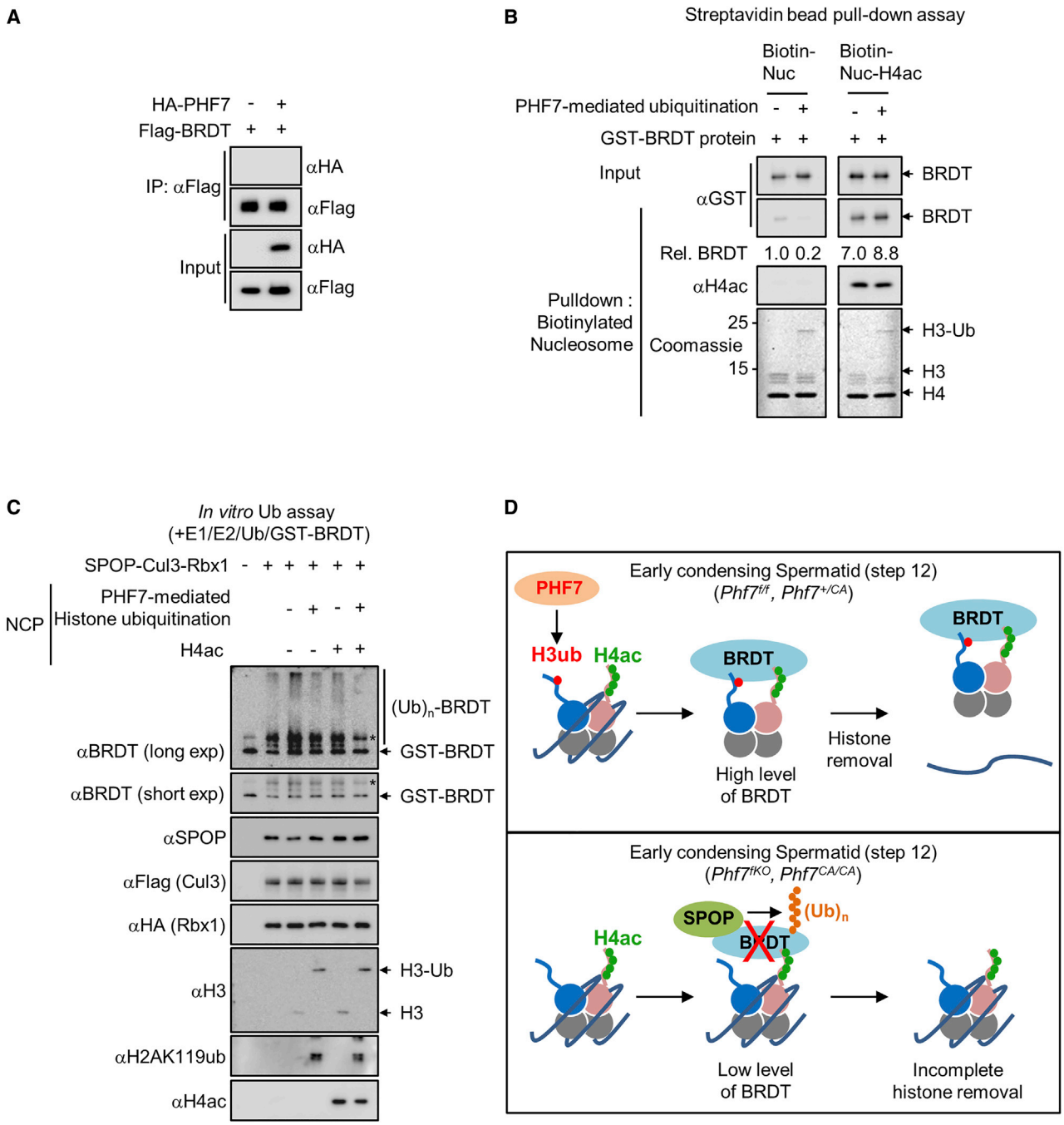

Figure 7. PHF7-Mediated Histone Ubiquitination Attenuates the Ubiquitination of BRDT

(A) Co-immunoprecipitation of BRDT with PHF7 from HEK293T cells.

(B) *In vitro* pull-down assay of biotinylated nucleosome bearing H3ub and/or H4ac with GST-BRDT from *E. coli* using streptavidin beads. Relative ratio of pulled down GST-BRDT was indicated below immunoblot.

(C) *In vitro* ubiquitination assay was performed with BRDT, SPOP-Cul3-Rbx1, and modified nucleosome.

(D) Schematic model showing regulation of BRDT stability via PHF7-mediated H3ub in early condensing spermatids (step 12).

- ○ Isolation of mouse testicular cells
- ○ Immunohistochemistry
- ○ Transfection and cell lysis
- ○ *In vitro* ubiquitination assay
- ○ *In vivo* ubiquitination assay
- ○ Immunoprecipitation

- *In vitro* biotin-streptavidin pull-down assay
- LC-MS/MS analysis
- Quantitative RT-PCR
- Single-cell RNA-seq experiment
- Single-cell RNA-seq data analysis

● QUANTIFICATION AND STATISTICAL ANALYSIS

SUPPLEMENTAL INFORMATION

Supplemental Information can be found online at https://doi.org/10.1016/j.celrep.2020.107950.

ACKNOWLEDGMENTS

We thank members of the Epigenetic Code and Diseases Research Center for discussions and technical assistance. This work was supported by Creative Research Initiatives Program (Research Center for Epigenetics Code and Diseases, grant NRF-2017R1A3B1023387 to S.H.B.); the Science Research Center program (grant NRF-2016R1A5A1010764 to S.H.B.); Korea University (grant K1925011 to H.K.); the Institute for Basic Science (grant IBS-R008-D1 to J.-S.K.); Korean Ministry of Health and Welfare, funded by the Korean Government (grant HI17C0328 to I.J.); and Ministry of Education, Culture, Sports, Science, and Technology (MEXT)/Japan Society for the Promotion of Science (JSPS) KAKENHI grants (JP18K14612 to T.N., JP19J21619 to S.O., JP17K17852 to K.S., and 19H05750 to M.I.). *Phf7*-floxed mouse was kindly provided from the Korea Mouse Phenotyping Center.

AUTHOR CONTRIBUTIONS

C.R.K., T.N., Y.O., M.I., and S.H.B. designed the experiments; C.R.K., T.N., G.K., H.L., and M.I. generated and maintained $Phf7^{f/f}$, $Phf7^{tKO}$, $Phf7^{C160A}$, and $Phf7^{FLAG}$ mice; C.R.K., T.N., S.O., and K.S. analyzed mouse phenotype; C.R.K., T.N., J.-Y.A., and S.K.O. performed histological assays; C.R.K., H.K., G.K., and Y.R.K. performed the cell biology and biochemistry experiments; C.R.K., S.P., and I.J. performed single-cell RNA sequencing analysis; Y.N., I.B., and J.-S.K. performed LC-MS/MS analysis; I.B. and H.-J.C. produced recombinant E1 and PHF7 protein; C.R.K., T.N., I.J., M.I., and S.H.B. wrote the manuscript; all authors contributed to data analysis.

DECLARATION OF INTERESTS

The authors declare no competing interests.

Received: September 4, 2019
Revised: February 16, 2020
Accepted: July 2, 2020
Published: July 28, 2020

REFERENCES

Baba, A., Ohtake, F., Okuno, Y., Yokota, K., Okada, M., Imai, Y., Ni, M., Meyer, C.A., Igarashi, K., Kanno, J., et al. (2011). PKA-dependent regulation of the histone lysine demethylase complex PHF2-ARID5B. Nat. Cell Biol. *13*, 668–675.

Barral, S., Morozumi, Y., Tanaka, H., Montellier, E., Govin, J., de Dieuleveult, M., Charbonnier, G., Couté, Y., Puthier, D., Buchou, T., et al. (2017). Histone Variant H2A.L.2 Guides Transition Protein-Dependent Protamine Assembly in Male Germ Cells. Mol. Cell *66*, 89–101.e8.

Berkovits, B.D., and Wolgemuth, D.J. (2013). The role of the double bromodomain-containing BET genes during mammalian spermatogenesis. Curr. Top. Dev. Biol. *102*, 293–326.

Bryant, J.M., Meyer-Ficca, M.L., Dang, V.M., Berger, S.L., and Meyer, R.G. (2013). Separation of spermatogenic cell types using STA-PUT velocity sedimentation. J. Vis. Exp. *80*, 50648.

Butler, A., Hoffman, P., Smibert, P., Papalexi, E., and Satija, R. (2018). Integrating single-cell transcriptomic data across different conditions, technologies, and species. Nat. Biotechnol. *36*, 411–420.

Cai, L., Rothbart, S.B., Lu, R., Xu, B., Chen, W.Y., Tripathy, A., Rockowitz, S., Zheng, D., Patel, D.J., Allis, C.D., et al. (2013). An H3K36 methylation-engaging Tudor motif of polycomb-like proteins mediates PRC2 complex targeting. Mol. Cell *49*, 571–582.

Chitalia, V.C., Foy, R.L., Bachschmid, M.M., Zeng, L., Panchenko, M.V., Zhou, M.I., Bharti, A., Seldin, D.C., Lecker, S.H., Dominguez, I., and Cohen, H.T. (2008). Jade-1 inhibits Wnt signalling by ubiquitylating beta-catenin and mediates Wnt pathway inhibition by pVHL. Nat. Cell Biol. *10*, 1208–1216.

Cho, C., Willis, W.D., Goulding, E.H., Jung-Ha, H., Choi, Y.C., Hecht, N.B., and Eddy, E.M. (2001). Haploinsufficiency of protamine-1 or -2 causes infertility in mice. Nat. Genet. *28*, 82–86.

Dai, X., Gan, W., Li, X., Wang, S., Zhang, W., Huang, L., Liu, S., Zhong, Q., Guo, J., Zhang, J., et al. (2017). Prostate cancer-associated SPOP mutations confer resistance to BET inhibitors through stabilization of BRD4. Nat. Med. *23*, 1063–1071.

Dhar, S., Thota, A., and Rao, M.R. (2012). Insights into role of bromodomain, testis-specific (Brdt) in acetylated histone H4-dependent chromatin remodeling in mammalian spermiogenesis. J. Biol. Chem. *287*, 6387–6405.

Fujihara, Y., Kaseda, K., Inoue, N., Ikawa, M., and Okabe, M. (2013). Production of mouse pups from germline transmission-failed knockout chimeras. Transgenic Res. *22*, 195–200.

Gaucher, J., Boussouar, F., Montellier, E., Curtet, S., Buchou, T., Bertrand, S., Hery, P., Jounier, S., Depaux, A., Vitte, A.L., et al. (2012). Bromodomain-dependent stage-specific male genome programming by Brdt. EMBO J. *31*, 3809–3820.

Gou, L.T., Kang, J.Y., Dai, P., Wang, X., Li, F., Zhao, S., Zhang, M., Hua, M.M., Lu, Y., Zhu, Y., et al. (2017). Ubiquitination-Deficient Mutations in Human Piwi Cause Male Infertility by Impairing Histone-to-Protamine Exchange during Spermiogenesis. Cell *169*, 1090–1104.e13.

Goudarzi, A., Shiota, H., Rousseaux, S., and Khochbin, S. (2014). Genome-scale acetylation-dependent histone eviction during spermatogenesis. J. Mol. Biol. *426*, 3342–3349.

Goudarzi, A., Zhang, D., Huang, H., Barral, S., Kwon, O.K., Qi, S., Tang, Z., Buchou, T., Vitte, A.L., He, T., et al. (2016). Dynamic Competing Histone H4 K5K8 Acetylation and Butyrylation Are Hallmarks of Highly Active Gene Promoters. Mol. Cell *62*, 169–180.

Green, C.D., Ma, Q., Manske, G.L., Shami, A.N., Zheng, X., Marini, S., Moritz, L., Sultan, C., Gurczynski, S.J., Moore, B.B., et al. (2018). A Comprehensive Roadmap of Murine Spermatogenesis Defined by Single-Cell RNA-Seq. Dev. Cell *46*, 651–667.e10.

Griswold, M.D. (2016). Spermatogenesis: The Commitment to Meiosis. Physiol. Rev. *96*, 1–17.

Han, X., Gui, B., Xiong, C., Zhao, L., Liang, J., Sun, L., Yang, X., Yu, W., Si, W., Yan, R., et al. (2014). Destabilizing LSD1 by Jade-2 promotes neurogenesis: an antibraking system in neural development. Mol. Cell *55*, 482–494.

Hermann, B.P., Cheng, K., Singh, A., Roa-De La Cruz, L., Mutoji, K.N., Chen, I.C., Gildersleeve, H., Lehle, J.D., Mayo, M., Westernströer, B., et al. (2018). The mammalian spermatogenesis single-cell transcriptome, from spermatogonial stem cells to spermatids. Cell Rep. *25*, 1650–1667.e8.

Janouskova, H., El Tekle, G., Bellini, E., Udeshi, N.D., Rinaldi, A., Ulbricht, A., Bernasocchi, T., Civenni, G., Losa, M., Svinkina, T., et al. (2017). Opposing effects of cancer-type-specific SPOP mutants on BET protein degradation and sensitivity to BET inhibitors. Nat. Med. *23*, 1046–1054.

Kim, S., and Pevzner, P.A. (2014). MS-GF+ makes progress towards a universal database search tool for proteomics. Nat. Commun. *5*, 5277.

Lee, M., Kim, I.S., Park, K.C., Kim, J.S., Baek, S.H., and Kim, K.I. (2017). Mitosis-specific phosphorylation of Mis18α by Aurora B kinase enhances kinetochore recruitment of polo-like kinase 1. Oncotarget *9*, 1563–1576.

Li, G., Ci, W., Karmakar, S., Chen, K., Dhar, R., Fan, Z., Guo, Z., Zhang, J., Ke, Y., Wang, L., et al. (2014a). SPOP promotes tumorigenesis by acting as a key regulatory hub in kidney cancer. Cancer Cell *25*, 455–468.

Li, W., Wu, J., Kim, S.Y., Zhao, M., Hearn, S.A., Zhang, M.Q., Meistrich, M.L., and Mills, A.A. (2014b). Chd5 orchestrates chromatin remodelling during sperm development. Nat. Commun. *5*, 3812.

Liu, W., Tanasa, B., Tyurina, O.V., Zhou, T.Y., Gassmann, R., Liu, W.T., Ohgi, K.A., Benner, C., Garcia-Bassets, I., Aggarwal, A.K., et al. (2010). PHF8 mediates histone H4 lysine 20 demethylation events involved in cell cycle progression. Nature *466*, 508–512.

Lu, L.Y., Wu, J., Ye, L., Gavrilina, G.B., Saunders, T.L., and Yu, X. (2010). RNF8-dependent histone modifications regulate nucleosome removal during spermatogenesis. Dev. Cell *18*, 371–384.

Matsumura, T., Noda, T., Muratani, M., Okada, R., Yamane, M., Isotani, A., Kudo, T., Takahashi, S., and Ikawa, M. (2019). Male mice, caged in the International Space Station for 35 days, sire healthy offspring. Sci. Rep. *9*, 13733.

Matzuk, M.M., McKeown, M.R., Filippakopoulos, P., Li, Q., Ma, L., Agno, J.E., Lemieux, M.E., Picaud, S., Yu, R.N., Qi, J., et al. (2012). Small-molecule inhibition of BRDT for male contraception. Cell *150*, 673–684.

Miller, T.C., Simon, B., Rybin, V., Grötsch, H., Curtet, S., Khochbin, S., Carlomagno, T., and Müller, C.W. (2016). A bromodomain-DNA interaction facilitates acetylation-dependent bivalent nucleosome recognition by the BET protein BRDT. Nat. Commun. *7*, 13855.

Morinière, J., Rousseaux, S., Steuerwald, U., Soler-López, M., Curtet, S., Vitte, A.L., Govin, J., Gaucher, J., Sadoul, K., Hart, D.J., et al. (2009). Cooperative binding of two acetylation marks on a histone tail by a single bromodomain. Nature *461*, 664–668.

Noda, T., Oji, A., and Ikawa, M. (2017). Genome Editing in Mouse Zygotes and Embryonic Stem Cells by Introducing SgRNA/Cas9 Expressing Plasmids. Methods Mol. Biol. *1630*, 67–80.

Noda, T., Sakurai, N., Nozawa, K., Kobayashi, S., Devlin, D.J., Matzuk, M.M., and Ikawa, M. (2019). Nine genes abundantly expressed in the epididymis are not essential for male fecundity in mice. Andrology *7*, 644–653.

Oji, A., Noda, T., Fujihara, Y., Miyata, H., Kim, Y.J., Muto, M., Nozawa, K., Matsumura, T., Isotani, A., and Ikawa, M. (2016). CRISPR/Cas9 mediated genome editing in ES cells and its application for chimeric analysis in mice. Sci. Rep. *6*, 31666.

Okada, Y., Scott, G., Ray, M.K., Mishina, Y., and Zhang, Y. (2007). Histone demethylase JHDM2A is critical for Tnp1 and Prm1 transcription and spermatogenesis. Nature *450*, 119–123.

Pivot-Pajot, C., Caron, C., Govin, J., Vion, A., Rousseaux, S., and Khochbin, S. (2003). Acetylation-dependent chromatin reorganization by BRDT, a testis-specific bromodomain-containing protein. Mol. Cell. Biol. *23*, 5354–5365.

Qi, H.H., Sarkissian, M., Hu, G.Q., Wang, Z., Bhattacharjee, A., Gordon, D.B., Gonzales, M., Lan, F., Ongusaha, P.P., Huarte, M., et al. (2010). Histone H4K20/H3K9 demethylase PHF8 regulates zebrafish brain and craniofacial development. Nature *466*, 503–507.

Qian, M.X., Pang, Y., Liu, C.H., Haratake, K., Du, B.Y., Ji, D.Y., Wang, G.F., Zhu, Q.Q., Song, W., Yu, Y., et al. (2013). Acetylation-mediated proteasomal degradation of core histones during DNA repair and spermatogenesis. Cell *153*, 1012–1024.

Sasaki, K., Ito, T., Nishino, N., Khochbin, S., and Yoshida, M. (2009). Real-time imaging of histone H4 hyperacetylation in living cells. Proc. Natl. Acad. Sci. USA *106*, 16257–16262.

Schindelin, J., Arganda-Carreras, I., Frise, E., Kaynig, V., Longair, M., Pietzsch, T., Preibisch, S., Rueden, C., Saalfeld, S., Schmid, B., et al. (2012). Fiji: an open-source platform for biological-image analysis. Nat. Methods *9*, 676–682.

Shang, E., Nickerson, H.D., Wen, D., Wang, X., and Wolgemuth, D.J. (2007). The first bromodomain of Brdt, a testis-specific member of the BET sub-family of double-bromodomain-containing proteins, is essential for male germ cell differentiation. Development *134*, 3507–3515.

Shapiro-Kulnane, L., Smolko, A.E., and Salz, H.K. (2015). Maintenance of Drosophila germline stem cell sexual identity in oogenesis and tumorigenesis. Development *142*, 1073–1082.

Shiota, H., Barral, S., Buchou, T., Tan, M., Couté, Y., Charbonnier, G., Reynoird, N., Boussouar, F., Gérard, M., Zhu, M., et al. (2018). Nut Directs p300-Dependent, Genome-Wide H4 Hyperacetylation in Male Germ Cells. Cell Rep. *24*, 3477–3487.e6.

Shirakata, Y., Hiradate, Y., Inoue, H., Sato, E., and Tanemura, K. (2014). Histone h4 modification during mouse spermatogenesis. J. Reprod. Dev. *60*, 383–387.

Sin, H.S., Barski, A., Zhang, F., Kartashov, A.V., Nussenzweig, A., Chen, J., Andreassen, P.R., and Namekawa, S.H. (2012). RNF8 regulates active epigenetic modifications and escape gene activation from inactive sex chromosomes in post-meiotic spermatids. Genes Dev. *26*, 2737–2748.

Toyoda, Y., Yokoyama, M., and Hosi, T. (1971). Studies on the fertilization of mouse eggs in vitro. II. Effects of in vitro pre-incubation of spermatozoa on time of sperm penetration of mouse eggs in vitro. Jpn. J. Anim. Reprod. *16*, 152–157.

Tyanova, S., Temu, T., and Cox, J. (2016). The MaxQuant computational platform for mass spectrometry-based shotgun proteomics. Nat. Protoc. *11*, 2301–2319.

Udeshi, N.D., Mertins, P., Svinkina, T., and Carr, S.A. (2013). Large-scale identification of ubiquitination sites by mass spectrometry. Nat. Protoc. *8*, 1950–1960.

Wang, L., and Wolgemuth, D.J. (2016). BET Protein BRDT Complexes With HDAC1, PRMT5, and TRIM28 and Functions in Transcriptional Repression During Spermatogenesis. J. Cell. Biochem. *117*, 1429–1438.

Wang, H., Zhao, R., Guo, C., Jiang, S., Yang, J., Xu, Y., Liu, Y., Fan, L., Xiong, W., Ma, J., et al. (2016). Knockout of BRD7 results in impaired spermatogenesis and male infertility. Sci. Rep. *6*, 21776.

Wang, T., Gao, H., Li, W., and Liu, C. (2019a). Essential Role of Histone Replacement and Modifications in Male Fertility. Front. Genet. *10*, 962.

Wang, X., Kang, J.Y., Wei, L., Yang, X., Sun, H., Yang, S., Lu, L., Yan, M., Bai, M., Chen, Y., et al. (2019b). PHF7 is a novel histone H2A E3 ligase prior to histone-to-protamine exchange during spermiogenesis. Development *146*, dev175547.

Wen, H., Li, J., Song, T., Lu, M., Kan, P.Y., Lee, M.G., Sha, B., and Shi, X. (2010). Recognition of histone H3K4 trimethylation by the plant homeodomain of PHF2 modulates histone demethylation. J. Biol. Chem. *285*, 9322–9326.

Xia, X., Cai, H., Qin, S., and Xu, C. (2012). Histone acetylase inhibitor curcumin impairs mouse spermiogenesis-an in vitro study. PLoS ONE *7*, e48673.

Yang, S.Y., Baxter, E.M., and Van Doren, M. (2012). Phf7 controls male sex determination in the Drosophila germline. Dev. Cell *22*, 1041–1051.

Yang, S.Y., Chang, Y.C., Wan, Y.H., Whitworth, C., Baxter, E.M., Primus, S., Pi, H., and Van Doren, M. (2017). Control of a Novel Spermatocyte-Promoting Factor by the Male Germline Sex Determination Factor PHF7 of *Drosophila melanogaster*. Genetics *206*, 1939–1949.

Zhang, P., Wang, D., Zhao, Y., Ren, S., Gao, K., Ye, Z., Wang, S., Pan, C.W., Zhu, Y., Yan, Y., et al. (2017). Intrinsic BET inhibitor resistance in SPOP-mutated prostate cancer is mediated by BET protein stabilization and AKT-mTORC1 activation. Nat. Med. *23*, 1055–1062.

Zhuang, T., Hess, R.A., Kolla, V., Higashi, M., Raabe, T.D., and Brodeur, G.M. (2014). CHD5 is required for spermiogenesis and chromatin condensation. Mech. Dev. *131*, 35–46.

STAR★METHODS

KEY RESOURCES TABLE

REAGENT or RESOURCE	SOURCE	IDENTIFIER
Antibodies		
Rabbit polyclonal anti-PHF7	Sigma-Aldrich	HPA070305; RRID:AB_2686248
Mouse monoclonal anti-Flag	Sigma-Aldrich	F3165; RRID:AB_259529
Mouse monoclonal anti-β-actin	Sigma-Aldrich	A1978; RRID:AB_476692
Rabbit polyclonal anti-H3	Abcam	ab1791; RRID:AB_302613
Rabbit polyclonal anti-H2A	Abcam	ab18255; RRID:AB_470265
Rabbit polyclonal anti-H2B	Abcam	ab1790; RRID:AB_302612
Rabbit polyclonal anti-TH2B	Abcam	ab23913; RRID:AB_2118143
Rabbit polyclonal anti-SPOP	Abcam	ab81163; RRID:AB_1641021
Rabbit polyclonal anti-Cul3	Abcam	ab1871; RRID:AB_302643
Mouse monoclonal anti-TNP2	Santa Cruz	sc-393843; RRID:N/A
Goat polyclonal anti-PRM2	Santa Cruz	sc-23104; RRID:AB_2284440
Rabbit polyclonal anti-GST	Santa Cruz	sc-459; RRID:AB_631586
Mouse monoclonal anti-PTEN	Santa Cruz	sc-7974; RRID:AB_628187
Rabbit monoclonal anti-H3 (17H2L9)	Thermo Fisher	Cat#702023 (ICC); RRID:AB_2532514
Rabbit monoclonal anti-H4 (D2X4V)	Cell Signaling Technology	Cat#13919; RRID:AB_2798345
Rabbit polyclonal anti-H4ac	Millipore	Cat#06-866; RRID:AB_310270
Mouse monoclonal anti-H2AK119ub (E6C5)	Millipore	Cat#05-678; RRID:AB_309899
Rabbit polyclonal anti-BRDT	Millipore	ABE432 (IHC); RRID:N/A
Rabbit polyclonal anti-BRDT	GeneTex	GTX100201 (*in vivo*); RRID:AB_1240521
Rabbit polyclonal anti-BRDT	Biovision	Cat#6643 (*in vitro*); RRID:N/A
Rabbit polyclonal anti-TNP1	Proteintech	Cat#17178-1-AP; RRID:AB_2206757
Mouse monoclonal anti-H2BK120ub	Active Motif	Cat#39623; RRID:AB_2793279
Mouse monoclonal anti-PRM1	Briar Patch Biosciences	Mab-Hup1M; RRID:N/A
Mouse monoclonal anti-PRM2	Briar Patch Biosciences	Mab-Hup2B (IHC); RRID:N/A

(*Continued on next page*)

Continued

REAGENT or RESOURCE	SOURCE	IDENTIFIER
Rabbit monoclonal anti-ubiquitin (FK2)	StressMarq Biosciences	SMC-550D; RRID:AB_2728859
Rabbit polyclonal anti-BRD4	Bethyl Laboratories	A301-985A; RRID:AB_1576498
Mouse monoclonal anti-HA	Covance	MMS-101R; RRID:AB_291263
Rabbit polyclonal anti-Tubulin	AbFrontier	LF-PA0146A; RRID:N/A
Mouse monoclonal anti-Xpress	Invitrogen	R910-25; RRID:AB_2556552
Bacterial and Virus Strains		
DH5-α *Escherichia coli*	Enzynomics	CP010
Rossetta *Escherichia coli*	Novagen	70954-3CN
Chemicals, Peptides, and Recombinant Proteins		
TOPreal qPCR 2X PreMIX	Enzynomics	RT500
MG132	A.G. Scientific	M-1157
DMSO (Vehicle)	Sigma-Aldrich	D2650
3X Flag peptide	Sigma-Aldrich	F4799
cOmplete Protease Inhibitor Cocktail	Roche	Cat#11697498001
TALON Metal Affinity Resin	Clontech	Cat#635501
Streptavidin agarose	Thermo Fisher	Cat#20353
Glutathion Sepharose High Performance	GE healthcare	Cat#17-5279-01
UbcH5a	BostonBiochem	E2-616
UbcH5b	BostonBiochem	E2-622
UbcH5c	BostonBiochem	E2-627
UbcH13/Ube1a	BostonBiochem	E2-664
Ubiquitin	BostonBiochem	U-100H
Biotinylated nucleosome	Epi Cypher	Cat#16-0006
Biotinylated H4ac nucleosome	Epi Cypher	Cat#16-0313
His-UBE1 protein (His-tagged purification)	This paper	N/A
GST-PHF7 protein (GST purification)	This paper	N/A
GST-BRDT protein (GST purification)	This paper	N/A
His-SPOP protein (His-tagged purification)	This paper	N/A
Flag-Cul3 / HA-Rbx1 protein (Flag-tagged purification)	This paper	N/A
Critical Commercial Assays		
PTMSCan Ubiquitin Remnant Motif (K-ε-GG) Kit	Cell Signaling Technology	Cat#14482
Orbitrap Fusion Lumos mass spectrometer	Thermo Fisher	IQLAAEGAAPFADBMBHQ
Chromium Single Cell 3′ Library & Gel Bead Kit v2	10X Genomics	PN-120237
Chromium Single Cell A Chip Kit	10X Genomics	PN-1000009
Chromium i7 Multiplex Kit	10X Genomics	PN-120262
NextSeq 500/550 Mid-Output v2.5 Kit (150 cycles)	Illumina	Cat#20024904
NovaSeq 6000 S4 Reagent Kit (300 cycles)	Illumina	Cat#20012866
Deposited Data		
Raw and analyzed data	This paper	GEO: GSE136752
Raw data	Mendeleys	https://doi.org/10.17632/7h6grmkwhg.1
Experimental Models: Cell Lines		
HEK293T cells	ATCC	CRL-11268 RRID:CVCL_1926

(*Continued on next page*)

Continued

REAGENT or RESOURCE	SOURCE	IDENTIFIER
Experimental Models: Organisms/Strains		
Mouse: C57BL/6J male	KOATECH	B601-110
Mouse: Tg(Stra8-icre)1Reb/J	Jackson Laboratory	Stock#008208 RRID:IMSR_JAX:008208
Mouse *: Phf7^{flox}* conditional knock-out C57BL/6J	This paper	N/A
Mouse *:* STOCK Phf7 < em2(C160A)Osb > Tg(CAG/Acr-EGFP)C3-N01-FJ002Osb	This paper	RBRC# 11032, CARD# 2939
Mouse *:* C57BL/6J-Phf7 < em3(FLAG/Phf7)Osb >	This paper	RBRC# 11056, CARD# 2963
Oligonucleotides		
mouse *Phf7* Forward: 5′-TGCAACAACCGAGAAGAGTTC-3′	This paper	N/A
mouse *Phf7* Reverse: 5′-CCTTGCTCATACAGACAGATGG-3′	This paper	N/A
mouse *Tnp1* Forward: 5′-GAGAGGTGGAAGCAAGAGAAAA-3′	Okada et al., 2007	N/A
mouse *Tnp1* Reverse: 5′-CCCACTCTGATAGGATCTTTGG-3′	Okada et al., 2007	N/A
mouse *Tnp2* Forward: 5′-GAAGGGAAAGTGAGCAAGAGAA-3′	Okada et al., 2007	N/A
mouse *Tnp2* Reverse: 5′-GCATAGAAATTGCTGCAGTGAC-3′	Okada et al., 2007	N/A
mouse *Prm1* Forward: 5′-ACAAAATTCCACCTGCTCACA-3′	Okada et al., 2007	N/A
mouse *Prm1* Reverse: 5′-GTTTTTCATCGGCGGTGGC-3′	Okada et al., 2007	N/A
mouse *Prm2* Forward: 5′-GCTGCTCTCGTAAGAGGCTACA-3′	Okada et al., 2007	N/A
mouse *Prm2* Reverse: 5′-AGTGATGGTGCCTCCTACATTT −3′	Okada et al., 2007	N/A
mouse *Brdt* Forward: 5′-AGTGGGCGGTTGACGAATC-3′	This paper	N/A
mouse *Brdt* Reverse: 5′-AGTCAGGCAGCTTTAGTTTCAC-3′	This paper	N/A
Recombinant DNA		
Plasmids: p3xFlag-CMV10-PHF7 WT and its mutants	This paper	N/A
Plasmids: pcDNA3-HA-PHF7 WT and C160A	This paper	N/A
Plasmids: pcDNA3-PHF7	This paper	N/A
Plasmids: GST-PHF7 WT and its mutants	This paper	N/A
Plasmids: pcDNA4-Hismax-Ub	This paper	N/A
Plasmids: pcDNA3-H3 WT-Flag and its mutants	This paper	N/A
Plasmids: GST-H3 WT and its mutants	This paper	N/A
Plasmids: p3xFlag-CMV10-BRDT 1-555 WT and ΔD	This paper	N/A
Plasmids: GST-BRDT 1-555	This paper	N/A
Plasmids: pcDNA3-SPOP	This paper	N/A
Plasmids: pcDNA3-HA-SPOP	This paper	N/A
Plasmids: p3xFlag-CMV10-Cul3	This paper	N/A
Plasmids: pcDNA3-HA-Rbx1	This paper	N/A
Plasmids: pET28a-His-SPOP	This paper	N/A
Software and Algorithms		
ImageJ/Fiji	Schindelin et al., 2012	https://fiji.sc/
GraphPad Prism 5	GraphPad software	N/A

(*Continued on next page*)

Continued

REAGENT or RESOURCE	SOURCE	IDENTIFIER
Computer-assisted sperm analysis (CASA) system (CEROS II)	Hamilton Thorne Biosciences	https://www.hamiltonthorne.com/index.php/products/casa-products/sperm-analysis-systems-research/ceros
MS-GF+ algorithm	Kim and Pevzner, 2014	https://omics.pnl.gov/software/ms-gf
MaxQuant software	Tyanova et al., 2016	https://www.maxquant.org/
Qual Browser software	Thermo Fisher	XCALI-97209
Cellranger v3.0.2	10X Genomics	https://www.10xgenomics.com/
Seurat v3.1.5	Butler et al., 2018	https://satijalab.org/seurat/

RESOURCE AVAILABILITY

Lead Contact

Further information and requests for reagents may be directed to and will be fulfilled by the Lead Contact, Sung Hee Baek (sbaek@snu.ac.kr).

Materials Availability

Mouse lines and plasmids generated in this study are available from the Lead Contact with a completed Materials Transfer Agreement.

Data and Code Availability

The single cell RNA sequencing datasets for mouse testicular cells generated during this study are available at GEO: GSE136752 GEO136752. Original data of immunoblot and immunohistochemistry have been deposited to Mendeley Data: https://doi.org/10.17632/7h6grmkwhg.1

EXPERIMENTAL MODEL AND SUBJECT DETAILS

Generation of Phf7 conditional knock-out mice

Three ES cell clones with the first allele deletion (tm1a) of *Phf7* were received from IMPC (International Mouse Phenotyping Consortium) and microinjected to C57BL/6 blastocytes. To remove the lacZ and neomycin cassette, heterozygous F1 was crossed with Flp deleter strain (FLPeR mice, The Jackson Laboratory strain 003946). The mice were crossed with Stra8-Cre mice (The Jackson Laboratory strain 008208) to generate testis-specific *Phf7*-deficient mice. Male $Phf7^{f/f}$ and $Phf7^{tKO}$ mice were sacrificed at the over 8 weeks of age. Genotyping primers for floxed alleles were as follows:

Forward 5′-ATCAGTGTGTCCAGAACTTCCATC-3′
Reverse 5′-TTATC GAGTGGAGGGACAGATGTG-3′.

All animal studies and procedures were approved by the Institutional Animal Care and Use Committee (IACUC) of Seoul National University.

Generation of Phf7 C160A knock-in mice and Flag-tagged Phf7 knock-in mice

Phf7 C160A KI mice were generated by transfecting ES cells with single guide RNA (sgRNA)/Cas9 expressing plasmids as described previously (Noda et al., 2017; Oji et al., 2016). Specifically, ES cells, EGR-G01 [129S2 × C57BL/6NCr-Tg(*CAG/Acr-Egfp*), (Fujihara et al., 2013) were used for genome editing. The target sequence of sgRNA was: 5′-GAACATCCACCAGGGGAGTT-3′. The HDR donor plasmid (pBluescript II SK (+) vector) was designed to introduce point mutation (TGT→GCT, C160A) in the seventh exon of *Phf7*. Chimeric progenies bearing C160A allele were crossed with wild-type B6D2F1 mice to generate heterozygous ($Phf7^{+/CA}$) mice. Then, $Phf7^{+/CA}$ mice were backcrossed withC57BL/6J mice. $Phf7^{CA/CA}$ mice were generated by cross between two $Phf7^{+/CA}$ mice. Male $Phf7^{+/CA}$ and $Phf7^{CA/CA}$ mice were sacrificed at the over 8 weeks of age. Genotyping primers for C160A alleles were as follows:

Forward; 5′- TCACTGAGCACCAAGCAAATAGAC-3′
Reverse; 5′- TCTGAATCTTACACATACTTGAGCA-3′.

As the KI allele has the recognition site for AfeI (Figure 3E), the genotype was distinguished by AfeI digestion. Flag-tagged *Phf7* KI mice were generated by injecting the mixture of gRNA/Cas9 ribonucleoprotein and reference DNA into oocytes as described previously (Noda et al., 2019). The gRNA sequence was 5′-AAAACAAACATCCAAGATTG-3′. Genotyping primers for Flag-*Phf7* alleles were as follows:

Forward 5′- GGGTGGGACGACAAGAAGAG −3′
Reverse 5′- CTTGTCATCGTCATCCTTGT −3′.

All animal studies and procedures were approved by the Institutional Animal Care and Use Committee (IACUC) of Seoul National University and the Animal Care and Use Committee of the Research Institute for Microbial Diseases, Osaka University. Frozen spermatozoa from these KI mice (STOCK Phf7 < em2(C160A)Osb > Tg(CAG/Acr-EGFP)C3-N01-FJ002Osb, RBRC#11032, CARD#2939; and C57BL/6J-Phf7 < em3(FLAG/Phf7)Osb >, RBRC#11056, CARD#2963) will be available through RIKEN BRC (https://mus.brc.riken.jp/en/) and the CARD, Kumamoto University (http://card.medic.kumamoto-u.ac.jp/card/english/).

Cell culture

HEK293T cells (ATCC) were cultured at 37°C in Dulbecco's modified Eagle's medium (DMEM) containing 10% fetal bovine serum (FBS) and antibiotics in a humidified incubator with 5% CO_2. All cells used in the study were regularly tested for mycoplasma contamination.

METHOD DETAILS

Antibodies and reagents

The following commercially available antibodies were used: anti-PHF7 (HPA070305, 1:100 for IB), anti-Flag (F3165, 1:5000 for IB, 1:50 for IHC), anti-β-actin (A1978, 1:5000 for IB) from Sigma-Aldrich, anti-histone H3 (ab1791, 1:2500 for IB), anti-H2A (ab18255, 1:1000 for IB, 1:100 for ICC), anti-H2B (ab1790, 1:5000 for IB), anti-TH2B (ab23913, 1:2500 for IB, 1:200 for ICC), anti-SPOP (ab81163, 1:2000 for IB), and anti-Cul3 (ab1871, 1:1000 for IB) from Abcam; anti-TNP2 (B-2, sc-393843, 1:1000 for IB, 1:100 for IHC), anti-PRM2 (sc-23104, 1:2000 for IB), anti-GST (sc-459, 1:5000 for IB), anti-PTEN (sc-7974, 1:100 for IB) from Santa Cruz biotechnology; anti-H3 (17H2L9, #702023, 1:200 for ICC, 1:500 for IHC) from Thermo Fisher; anti-H4 (D2X4V, #13919, 1:1000 for IB, 1:100 for ICC) from Cell Signaling Technology; anti-H4ac (06-866, 1:2500 for IB, 1:500 for IHC), anti-H2AK119ub (05-678, 1:1000 for IB), and anti-BRDT (ABE432, 1:50 for IHC) from Millipore; anti-BRDT (GTX100201, 1:2500 for IB) from GeneTex; anti-BRDT (#6643, 1:1000 for IB) from Biovision; anti-TNP1 (#17178-1-AP, 1:2000 for IB) from Proteintech; anti-H2BK120ub (#39623, 1:1000 for IB) from Active Motif; anti-PRM1 (Mab-Hup1M-1000, 1:2500 for IB, 1:50 for IHC) and anti-PRM2 (Mab-Hup2B-150, 1:50 for IHC) from Briar Patch Bioscience; anti-Ub (FK2, SMC-550D) from StressMarq Biosciences; anti-BRD4 (A301-985A, 1:1000 for IB) from Bethyl Laboratories; anti-Xpress (R910-25, 1:5000 for IB) from Invitrogen; anti-HA (MMS-101R, 1:5000 for IB) from Covance; and anti-Tubulin (LF-PA0146A, 1:2500 for IB) from Abfrontier. The following commercially available reagents were used for *in vitro* assay: UbcH5a(E2-616), UbcH5b (E2-622), UbcH5c (E2-627), UbcH13/Ube1a (E2-664), and ubiquitin (U-100H) from Boston Biochem; Recombinant biotinylated nucleosome (16-0006) and H4ac recombinant nucleosome (16-0313) from Epi Cypher.

Sperm motility

Sperm were collected from cauda epididymis. Epididymal sperm were dispersed in TYH drops (Toyoda et al., 1971). After 10 min of incubation, the sperm motility was examined using the Computer-assisted sperm analysis (CASA) system (CEROS II) (Hamilton Thorne Biosciences) (Matsumura et al., 2019).

In vitro fertilization assay

Pregnant mare serum gonadotropin (PMSG) (5 units, ASKA Pharmaceutical) was injected into the abdominal cavity of B6D2F1 females, followed by human chorionic gonadotropin (hCG) (5 units, ASKA Pharmaceutical) 48 h after PMSG. Fourteen hr after hCG injection, oocytes were collected from ampulla of each oviduct, and then incubated into TYH drop. Cauda epididymal spermatozoa were pre-incubated in TYH drop for 2 hr. The sperm suspension was added to TYH drop with oocytes. After 6 hr of insemination, cumulus cells surrounding eggs were removed by treatment of hyaluronidase (final conc. 300 μg/mL) for 5 min, and then the pronuclei were observed under a phase contrast microscopy (Olympus).

Histology

The testis histology was performed as described previously (Noda et al., 2019). The epididymis was fixed in 10% formalin (Sigma) at 4°C overnight. After fixation, tissues were sequentially dehydrated in ethanol with increasing concentrations ranging from 50 to 100%. Dehydrated specimens were subsequently infiltrated with 100% xylene and embedded in paraffin wax. For hematoxylin and eosin (H&E) staining, tissues were sectioned at 7 μm-thickness, deparaffinized, rehydrated, and stained with hematoxylin for 3 min followed by counterstaining with eosin for 1 min. Images were acquired using digital microscopes (Leica DMD108, Leica microsystems)

Isolation of mouse testicular cells

Mouse testis tissues were digested with collagenase A (Roche), DNase I (Roche), and trypsin in DMEM-F12. Trypsin was blocked using FBS and cells were filtered using 70 μm and 40 μm strainers. Following centrifugation, red blood cells were removed using

RBC lysis buffer (eBioscience). Cells were washed with HBSS. Spermatids were isolated by STA-PUT, the unit gravity sedimentation, with modification from protocol described previously (Bryant et al., 2013). 2% BSA in DMEM-F12 medium was slowly stacked over 4% BSA in column and testicular cell suspension in 0.5% BSA was loaded over 2% BSA. The sedimentation was performed for 150 min at room temperature. Each fraction was distinguished by cell morphology with phase contrast microscope.

Immunohistochemistry

Sperm from cauda epididymis dried on slide and spermatids on PLL-treated coverslips were incubated with 1 M DTT in PBS for 30 min and then fixed with 4% PFA in PBS for 10 min at RT. Fixed samples were permeabilized with 0.1% Triton X-100 in PBS (PBS-T) for 10 min at RT. Blocking was performed with 10% FBS in PBS-T for 30 min. For staining, cells were incubated with antibodies for 2 hours at RT, followed by incubation with fluorescent labeled secondary antibodies for 1 hour (Invitrogen). Immunohistochemistry was performed using testis sections with the same method including steps from blocking to mounting. Samples were mounted and visualized under a confocal microscope (Zeiss, LSM700). For double-staining with two antibodies from the same host (rabbit), testis sections were incubated with anti-BRDT antibody (Sigma) at 4°C for overnight. Then, the incubation for 1 hr at RT was performed with following antibodies in order; Alexa 488 AffiniPure Fab Fragment Donkey Anti-Rabbit IgG (H+L) (Jackson Immuno Research), anti-H4ac antibody (Millipore), and Alexa 594 Donkey Anti-Rabbit IgG (H+L) (Invitrogen). Mounted samples were visualized under a confocal microscope (Leica, SP8).

Transfection and cell lysis

Transfection was performed with PEI (Sigma-Aldrich). All cells were briefly rinsed with ice-cold PBS before collection. The cells were lysed with Laemmli sample buffer. All lysates were analyzed by SDS-PAGE.

In vitro ubiquitination assay

Recombinant protein PHF7, UBE1, GST-H3, GST-BRDT, and His-SPOP were purified from the *E. coli* strain Rosetta. Histone ubiquitination assay using recombinant nucleosome, GST-H3, and histone extract was performed with ubiquitin, UBE1, UbcH5b, UbcH5c, and PHF7 in assay buffer (50 mM Tris-HCl [pH 7.5], 5 mM $MgCl_2$, 2 mM ATP, and 2 mM DTT) at 30°C for 1 hr. Flag-Cul3 and HA-Rbx1 protein were purified from transfected HEK293T cells using Flag-M2 agarose beads and 3xFlag peptide (Sigma-Aldrich). GST-BRDT, His-SPOP, Flag-Cul3, HA-Rbx1, and PHF7 were incubated in the same buffer at 30°C for 30 min and then BRDT ubiquitination assay was performed with incorporation of ubiquitin, UBE1, and UbcH5a at 30°C for 1 hr. Following ubiquitination assay with PHF7 and recombinant nucleosome, modified nucleosome was filtered to remove PHF7, ubiquitin, UbcH5b, and UbcH5c by Amicon Ultra Centrifugal Filters 50K membrane (Millipore). BRDT ubiquitination assay with modified nucleosome was performed using the same method.

In vivo ubiquitination assay

Testicular cells were lysed with denaturing buffer (50 mM Tris-HCl [pH 7.5], 1% SDS, and 70 mM β-mercaptoethanol) and boiled for 5 min at 95°C. After lysates were diluted with non-denaturing buffer (20 mM Tris-HCl [pH 7.5], 200 mM NaCl, 1 mM EGTA, 1 mM EDTA, 1% Triton X-100, and protease inhibitor), immunoprecipitation was performed with anti-H3 antibody at 4°C for overnight. HEK293T cells were transfected with plasmids including Hismax-Ub. Following MG132 (10 μg/ml) treatment for 6 hr, cells were lysed with the same way. Immunoprecipitation was performed with anti-Flag antibody at 4°C for 2 hr.

Immunoprecipitation

Transfected HEK293T cells were lysed with EBC200 buffer (50 mM Tris-HCl [pH 8.0], 200 mM NaCl, 0.5% NP-40, and protease inhibitor) and followed by centrifugation. Supernatant was incubated with anti-Flag antibody at 4°C for 2 hr. Then, protein A/G Sepharose beads were added and incubated at 4°C for 1 hr. The beads were washed with EBC200 buffer and boiled with sample buffer for 10 min.

In vitro biotin-streptavidin pull-down assay

Recombinant protein GST-BRDT was purified from the *E. coli* strain Rosetta. Recombinant biotinylated nucleosome was used in *in vitro* ubiquitination assay using PHF7, and then was incubated with Streptavidin agarose resin (Thermo Fisher) in pulldown buffer (50 mM Tris-HCl [pH 7.4], 125 mM KCl, 5 mM $MgCl_2$, 0.5mM EDTA, 0.5% Triton X-100, and 5mM DTT) at 4°C for 1 hr. Bead bound nucleosome was washed, and then incubated with GST-BRDT proteins in pulldown buffer at 4°C for 2 hr. The beads were washed and boiled for 10 min.

LC-MS/MS analysis

In-gel peptide sample preparation and subsequent LC-MS/MS analysis of the *in vitro* modified histone sample was largely done as described previously (Lee et al., 2017). Peptide sample preparations and immunoaffinity purifications of control and PHF7-overexpressing HEK293T cells and testicular cells from $Phf7^{f/f}$ and $Phf7^{tKO}$ mice were done, as described previously (Udeshi et al., 2013), using a PTMSCan Ubiquitin Remnant Motif (K-ε-GG) Kit (Cell Signaling Technology). Prepared peptide samples were separated on in-house packed long capillary columns (100 cm x 75 μm i.d.) and trap columns (3 cm x 150 μm i.d) with 3 μm Jupiter C18 particles

(Phenomenex). A flow rate of 300 nl/min and a linear gradient ranging from 95% solvent A (water with 0.1% formic acid) to 40% of solvent B (acetonitrile with 0.1% formic acid) for 60 min were applied on nanoACQUITY UPLC (Waters) coupled with Orbitrap Fusion Lumos mass spectrometer (Thermo Scientific), which was operated using the following parameters: m/z 300–1800 of precursor scan range, 1.4 Th of precursor isolation window, 30% of normalized collision energy (NCE) for higher-energy collisional dissociation (HCD), 30 s of dynamic exclusion duration, 60k or 7.5k resolution at m/z 200 for full MS or MS/MS scan, respectively. The acquired dataset was searched by MS-GF+ algorithm or MaxQuant software at 10 ppm of precursor ion mass tolerance (with carbamidomethylation of cysteine as static modification, acetylation and diGLY of lysine as variable modification), against the SwissProt *Homo sapiens* proteome database. A false discovery rate was set to 1% for both protein and peptide levels. (10 ppm search) The number of peptide spectrum match were counted for each identified peptide sequences. Intensities of the peptide sequences of interest were either obtained from MaxQuant search results or determined through the manual annotation of the extracted ion chromatogram (XIC) levels using Qual Browser software (Thermo).

Quantitative RT-PCR

Total RNAs were extracted using Trizol (Invitrogen) and reverse transcription was performed with 2.5 μg total RNAs using the M-MLV cDNA Synthesis kit (Enzynomics). The abundance of mRNA was detected by a BioRad CFX384 with SYBR TOPreal qPCR 2x PreMix (Enzynomics). The quantity of mRNA was calculated using ddCt method and all reactions were performed as triplicates. Expression was normalized using 18S rRNA and *Hprt*.

Single-cell RNA-seq experiment

Single-cell RNA-seq libraries were generated by the Chromium Single Cell 3′ Library & Gel Bead Kit v2. Briefly, thousands of testicular cells were separated into nano liter-scale droplets. In each droplet, cDNA was generated through reverse transcription reaction. As a result, barcode sequence and Unique Molecular Identifier (UMI) was added to each cDNA molecule. cDNA was pooled and libraries for sequencing were prepared as the manufacturer's instructions. The libraries were sequenced using Nextseq 550 platform and Novaseq 6000 platform.

Single-cell RNA-seq data analysis

The sequenced data was de-multiplexed using bcl2fastq (Illumina) to generate fastq files. After de-multiplexing, reads were aligned to the mouse reference genome (mm10; 10x cellranger reference mm10 v2.1.0) and feature-barcode matrices were made using cellranger count with trimming (–r1-length = 26,–r2-length = 75) and aggregated by cellranger aggr with default parameters. The following analysis was conducted using Seurat program. After generating feature-barcode matrix, we discarded genes which were expressed in less than 3 cells and cells that were expressing less than 200 genes. Furthermore, we exclude the cells showing over 20% of mitochondrial gene expression and expressing less than 2,000 molecules for further analysis. The data was normalized and scaled for dimension reduction method. To visualize the high dimension data, principle component analysis (PCA) was conducted with highly variable genes selected by FindVariableFeature with 'mean.var.plot'. The cells were assigned to distinct clusters using FindClusters with 10 PCs and 0.5 resolution parameter. Using UMAP, we embedded the cells based on 10 PCs then visualized it with the cell's cluster information.

QUANTIFICATION AND STATISTICAL ANALYSIS

The quantification of immunoblot was completed using ImageJ software. All experiments were reproduced at least three times. Statistical analysis was performed with Mann-Whitney U-tests and Student's t tests for group differences using GraphPad Prism software. The results of the statistical tests and the sample number (n) of experiments with mice were represented within the figure legends.